

The isotopic composition of rainfall on a subtropical mountainous island

Giuseppe Torri¹, Alison D. Nugent², and Brian N Popp²

¹University of Hawaii

²University of Hawaii at Manoa

November 22, 2022

Abstract

Tropical islands are simultaneously some of the most biodiverse and vulnerable places on Earth. Water resources help maintain the delicate balance on which the ecosystems and the population of tropical islands rely. Hydrogen and oxygen isotope analyses are a powerful tool in the study of the water cycle on tropical islands, although the scarcity of long-term and high-frequency data makes interpretation challenging. Here, a new dataset is presented based on weekly collection of rainfall H and O isotopic composition on the island of O‘ahu, Hawai‘i, beginning from July 2019 and still ongoing. Throughout this time, a variety of weather conditions have affected the island, each producing rainfall with different isotopic ratios: precipitation from Kona lows was found to have the lowest isotopic ratios, whereas trade-wind showers had the highest. These data also show some differences between the windward and the leeward side of the island, the latter being associated with higher rainfall isotope ratios due to increased rain evaporation. At all sites, the measured deuterium excess shows a marked seasonal cycle which is attributed to different origins of the air masses that are responsible for rainfall in the winter and summer months. The local meteoric water line is then determined and compared with similar lines for O‘ahu and other Hawaiian islands. Finally, a comparison is made with data collected on Hawai‘i Island for a longer period of time, and it is shown that the isotopic composition of rainfall exhibits significant interannual variability.

Abstract

Tropical islands are simultaneously some of the most biodiverse and vulnerable places on Earth. Water resources help maintain the delicate balance on which the ecosystems and the population of tropical islands rely. Hydrogen and oxygen isotope analyses are a powerful tool in the study of the water cycle on tropical islands, although the scarcity of long-term and high-frequency data makes interpretation challenging. Here, a new dataset is presented based on weekly collection of rainfall H and O isotopic composition on the island of O‘ahu, Hawai‘i, beginning from July 2019 and still ongoing. Throughout this time, a variety of weather conditions have affected the island, each producing rainfall with different isotopic ratios: precipitation from Kona lows was found to have the lowest isotopic ratios, whereas trade-wind showers had the highest. These data also show some differences between the windward and the leeward side of the island, the latter being associated with higher rainfall isotope ratios due to increased rain evaporation. At all sites, the measured deuterium excess shows a marked seasonal cycle which is attributed to different origins of the air masses that are responsible for rainfall in the winter and summer months. The local meteoric water line is then determined and compared with similar lines for O‘ahu and other Hawaiian islands. Finally, a comparison is made with data collected on Hawai‘i Island for a longer period of time, and it is shown that the isotopic composition of rainfall exhibits significant interannual variability.

Plain Language Summary

Water molecules come in different forms that contain atoms of slightly different weights, called isotopes. Knowledge about the ratio of various isotopes in a water sample can be used to study past climates and the water cycle in a given region. Here, a new 2-year dataset of water isotopic composition is presented that was collected on the island of O‘ahu, in the Hawaiian Archipelago. By comparing the data with the weather conditions during each collection period, the isotopic signature of various weather systems is presented, and it is shown that large-scale storms, called Kona lows, produce rain that has particularly low heavy-to-light isotope ratios. Differences are also found between the isotopic composition of rain fallen on the windward side of the island and that on the leeward side, and this was attributed to differences in rain evaporation rates. A parameter called deuterium excess is computed, and its seasonal variations are interpreted as a result of differences in the origin of the air masses contributing to precipitating systems in winter and summer months. Finally, significant interannual differences were observed, suggesting a potential correlation with large-scale modes of climate variability, although a longer dataset will be needed to investigate this in detail.

1 Introduction

Climate represents an important component of the delicate equilibrium on which the biodiverse ecosystems on tropical islands rest (Veron et al., 2019). As the world begins to deal with the consequences of a changing climate, tropical islands are especially vulnerable to how those changes will manifest themselves at a regional scale (Veron et al., 2019). For example, in Hawai‘i more than 99% of the fresh water supply comes from rainfall (Gingerich & Oki, 2000). Any disruption to the hydroclimate in the North Pacific region can therefore threaten the ecosystems and the habitability of the islands, which are currently home to more than a million people (U.S. Census Bureau, 2020). A better understanding of the climate of tropical islands is therefore a task of utmost importance.

In the study of climate, analyses of the stable isotopic composition of water are a particularly useful tool. Because slight mass differences provide them with different chemical and physical properties (Dansgaard, 1964), $\delta^2\text{H}$ and $\delta^{18}\text{O}$ values in water can be used

to infer where an air parcel originated from, the climatic conditions at the origin, or the microphysical processes that it underwent in its history (Dansgaard, 1964; Galewsky et al., 2016). This has led to many important insights in disciplines, including, for example, paleoclimatology (Woodruff et al., 1981; Bar-Matthews et al., 1997; Cruz et al., 2005; LeGrande & Schmidt, 2009; Yao et al., 2013; Yoshimura, 2015; Kontakiotis, 2016; Opel et al., 2018; Cluett & Thomas, 2020) and ecology (Ehleringer & Dawson, 1992; Dawson et al., 2002; Marshall et al., 2007; Lai & Ehleringer, 2011; Cai et al., 2015; Evaristo et al., 2016; Grossiord et al., 2017; Lovelock et al., 2017; Aron et al., 2019; Adkison et al., 2020; Timofeeva et al., 2020; Hahn et al., 2021; Tetzlaff et al., 2021).

In Hawai‘i, stable isotopes in water have been used in a variety of different contexts. In recent years, measurements of the isotopic composition of water vapor at the summit of Mauna Loa, on Hawai‘i Island, have been used to diagnose important processes in the tropical atmosphere (Galewsky et al., 2007; Gupta et al., 2009; Noone et al., 2011; Hurley et al., 2012; Bailey et al., 2013; Galewsky, 2018). As another example, in the study of the islands’ hydrology, the comparison between the isotopic composition of water found in springs and wells with that of rainfall has been used to determine flow paths and recharge areas for groundwater on different parts of Hawai‘i Island (Scholl et al., 1996; Tillman et al., 2014; Kelly & Glenn, 2015; Fackrell et al., 2020; Tachera et al., 2021), Maui (Scholl et al., 2002, 2007), and O‘ahu (Dores et al., 2020).

Most of the $\delta^{2}\text{H}$ and $\delta^{18}\text{O}$ values measured in water collected in Hawai‘i, however, are characterized by collection frequencies of the order of months. While these might be adequate to study processes involving groundwater aquifers, that occur over longer time scales compared to atmospheric phenomena, such long collection frequencies make interpretation of the data challenging. The longest available record of the isotopic composition of rainfall in Hawai‘i was collected with a monthly frequency between 1962 and 1970 as part of the Global Network of Isotopes in Precipitation (GNIP)(IAEA/WMO, 2021). However, the lack of reliable satellite data and the scarcity of other weather observations at the time make the interpretation of the isotope data equally challenging. The GNIP dataset also presented another limitation, because all the data were collected in a single location on the windward side of Hawai‘i Island, thus potentially introducing biases: for example, the same weather system coming from different directions would likely produce rain with different isotopic compositions thanks to the island orographic effect.

Here, a new dataset of $\delta^{2}\text{H}$ and $\delta^{18}\text{O}$ values of rainfall is presented. The data were collected on the island of O‘ahu with a weekly frequency over five different sites, two on the windward side and three on the leeward side. The data discussed here span two years, from July 2019 until July 2021, although collection is still ongoing. In Section 2, all the definitions and the data used for this study are introduced. In Section 3, the rainfall isotope dataset is presented and interpreted. In Section 4, the implications of the data are discussed. Finally, conclusions are presented in Section 5

2 Methods

2.1 Definitions

Throughout this manuscript, three stable water isotopologues are considered, $^1\text{H}_2\text{}^{16}\text{O}$, $^1\text{H}_2\text{}^{18}\text{O}$ and $^1\text{H}^2\text{H}^{18}\text{O}$. Isotopologues are referred to by the isotope that makes them different from the lighter isotopologue, $^1\text{H}_2\text{}^{16}\text{O}$: ^{18}O for $^1\text{H}_2\text{}^{18}\text{O}$ and ^2H for $^1\text{H}^2\text{H}^{18}\text{O}$. The isotope ratios of H and O are defined as the concentration of heavy isotope in a given sample divided by the concentration of the lighter isotope:

$$R_{18\text{O}} \equiv [^{18}\text{O}]/[^{16}\text{O}], \quad (1)$$

$$R_{2\text{H}} \equiv [^2\text{H}]/[^1\text{H}], \quad (2)$$

where the square brackets represent the concentration of an isotope. Isotope abundances are defined as

$$\delta X \equiv 1000 \times \left(\frac{R_X}{R_{VSMOW}} - 1 \right), \quad (3)$$

108 where R_{VSMOW} is the Vienna Standard Mean Ocean Water, and X indicates one of the
109 two heavier isotopes. The unit of measurement for isotopic abundances is ‰, or permil.

From the isotopic abundances, a second-order parameter, called deuterium excess, d , can be defined as:

$$d \equiv \delta^2\text{H} - 8 \times \delta^{18}\text{O}. \quad (4)$$

110 Deuterium excess has been shown to be particularly sensitive to environmental condi-
111 tions at the moisture source (Merlivat & Jouzel, 1979; Uemura et al., 2008; Pfahl & Sode-
112 mann, 2014), and it is thus often used as a diagnostic tool to investigate the origins of
113 air masses responsible for precipitation in a particular region (Vimeux et al., 1999; Masson-
114 Delmotte et al., 2005; Jouzel et al., 2007; Pfahl & Wernli, 2009; Pfahl & Sodemann, 2014).

The Global Meteoric Water Line (GMWL) is an empirical linear relationship between the H and O isotope abundances in water (Craig, 1961):

$$\delta^2\text{H} = 8 \times \delta^{18}\text{O} + 10\text{‰}. \quad (5)$$

115 While the GMWL was originally discovered by considering precipitation samples from
116 all over the world, more regional versions have also been used (Rozanski et al., 1993).
117 These, generally known as Local Meteoric Water Lines (LMWLs), represent the same
118 empirical relationship, except that the slope and intercept of the lines can be different
119 from the GMWL. Departures from the GMWL are typically linked to processes, like evap-
120 oration, that happen in a given region (Rozanski et al., 1993; Putman et al., 2019).

121 2.2 The Island of O‘ahu

122 O‘ahu is the third largest island of the Hawaiian Archipelago, a group of islands
123 and islets that extends for thousands of kilometers in the North Pacific region. The sur-
124 face area of O‘ahu covers approximately 1,544 km² and its topography has been shaped
125 by two separate shield volcanos: the remnants of the northernmost one constitute the
126 Ko‘olau Range, with a peak at 960 m called Pu‘u Kōnāhuanui; those of the southern-
127 most volcano form the Wai‘anae Range, its highest peak being Mount Ka‘ala with an
128 elevation of 1,220 m (*State of Hawaii Data Book*, 2004).

129 The climate of O‘ahu is divided in two main periods: a dry season, which, follow-
130 ing other studies (Longman et al., 2021), is here defined as the 6-month window between
131 May and October; and a wet season, that covers the remaining 6 months of the year. A
132 quasi-permanent high-pressure center located thousands of kilometers northeast of the
133 island strongly modulates its climate and is responsible for steady trade winds. These
134 have been estimated to blow over the Hawaiian Archipelago 50-80% of the time during
135 the wet season, and 85-95% during the dry season (Longman et al., 2021). The orographic
136 lifting provided to the moist air flow by the Ko‘olau and the Wai‘anae ranges on O‘ahu
137 causes cloud condensation and the formation of rain, most of which falls in the vicinity
138 of the mountain ranges (Giambelluca et al., 2013).

139 Trade wind showers are not the only weather systems responsible for rainfall on
140 O‘ahu (K. Kodama & Barnes, 1997; K. R. Kodama & Businger, 1998). During the wet
141 season, a considerable amount of rainfall is often generated in relatively short periods
142 of time by synoptic weather systems, such as cold fronts, upper-tropospheric troughs,
143 and subtropical storms, called Kona lows (Simpson, 1952). Tropical cyclones (TCs) also
144 contribute, although these typically occur during the dry season. In a recent study, Longman
145 et al. (2021) analyzed daily rainfall on O‘ahu during the period 1990-2010 and determined

146 that non-disturbance type rainfall caused by trade winds accounted for 70.6% of the to-
 147 tal rainfall amount during the 20-year window, cold fronts for 15.5%, Kona lows for 8.8%,
 148 upper-tropospheric lows for 3.6%, and TCs accounted only for 1.6%.

149 Interannual variability of rainfall in Hawai‘i is driven mainly by two large-scale modes
 150 (Chu & Chen, 2005). The first is known as the El Niño Southern Oscillation (ENSO)
 151 and it happens on temporal scales between 2 and 8 years (Trenberth, 1997). Its posi-
 152 tive phase, called El Niño, is characterized by an anomalous warming of the central/eastern
 153 parts of the tropical Pacific Ocean and a deepening of the Aleutian low. The second phe-
 154 nomenon is known as the Pacific Decadal Oscillation (PDO) (Mantua et al., 1997), and
 155 in its positive phase is characterized by colder sea surface temperatures (SSTs) in the
 156 Western Pacific Ocean, and warmer SSTs in the Central and Eastern Pacific Ocean. The
 157 PDO is characterized by longer frequencies than ENSO, single phases persisting some-
 158 times over 20 years or longer. In Hawai‘i, positive phases of ENSO tend to lead to lower
 159 rainfall amounts compared to the negative phases. Similarly, positive phases of the PDO
 160 are typically associated with drier conditions (Chu & Chen, 2005).

161 **2.3 Data**

162 *2.3.1 Isotope sites*

163 The rainwater collection network that was built to collect the data presented in this
 164 manuscript is made of five sites located on the island of O‘ahu. The locations of the col-
 165 lection sites were chosen to give the network a northeast-southwest orientation. Because
 166 this is approximately the direction along which trade winds blow, the network makes it
 167 possible to look at the evolution of the isotopic composition of trade-wind showers as they
 168 move across the island and over the Ko‘olau Range. Future expansions of the network
 169 are planned to include other locations on O‘ahu as well as on other islands in the Hawai-
 170 ian Archipelago.

171 On the windward side, the network is composed by two sites, one in the city of Kailua
 172 and the other in the residential district of Maunawili. On the leeward side, the site clos-
 173 est to the Ko‘olau Range is at Lyon Arboretum, followed to the south by another site
 174 at the Hawai‘i Institute of Geophysics (HIG) on the University of Hawai‘i at Mānoa cam-
 175 pus, and, finally, one in Waikīkī. A summary of the sites’ names, positions, and deploy-
 176 ment date is presented in Table 1. Collections of rainfall at Waikīkī, Lyon Arboretum,
 177 and HIG were made through a Palmex Rain Sampler 1, in which water enters through
 178 a cylinder measuring 13.5 cm in diameter and is deposited in a 3 L HDPE plastic bot-
 179 tle (Gröning et al., 2012). At Maunawili, collections were made through a Palmex Rain
 180 Sampler 2, which differs from the others only for its larger size and for the volume of the
 181 HDPE plastic bottles used (6/10 L instead of 3 L). In Kailua, rainfall was collected us-
 182 ing a 1-L separatory funnel fitted with a 13.0 cm diameter funnel and filled with approx-
 183 imately 50 mL heavy mineral oil to prevent evaporation.

184 Restrictions put in place because of the COVID-19 pandemic—as well as concerns
 185 about our own safety—made some collections particularly challenging: Lyon Arboretum
 186 was closed to the public for several weeks in March and April 2020. Heavy precipitation
 187 that fell during those weeks caused the rain sampler to overflow, and the data are con-
 188 sidered inaccurate. For similar reasons, data collection at Waikīkī was discontinued in
 189 March 2020, only a few months after the deployment of the rain sampler.

190 In addition to the collection in April 2020, there were a couple of other times when
 191 debris was found in the funnel of the rain sampler, which caused it to overflow. In turn,
 192 this could have affected the isotopic composition of the rain water: for example, the par-
 193 tial obstruction could have slowed down the flow of the water into the funnel, thus ex-
 194 posing it to additional evaporation when still in the funnel. While still reported in the
 195 figures in this manuscript, data from these collections are marked with crosses.

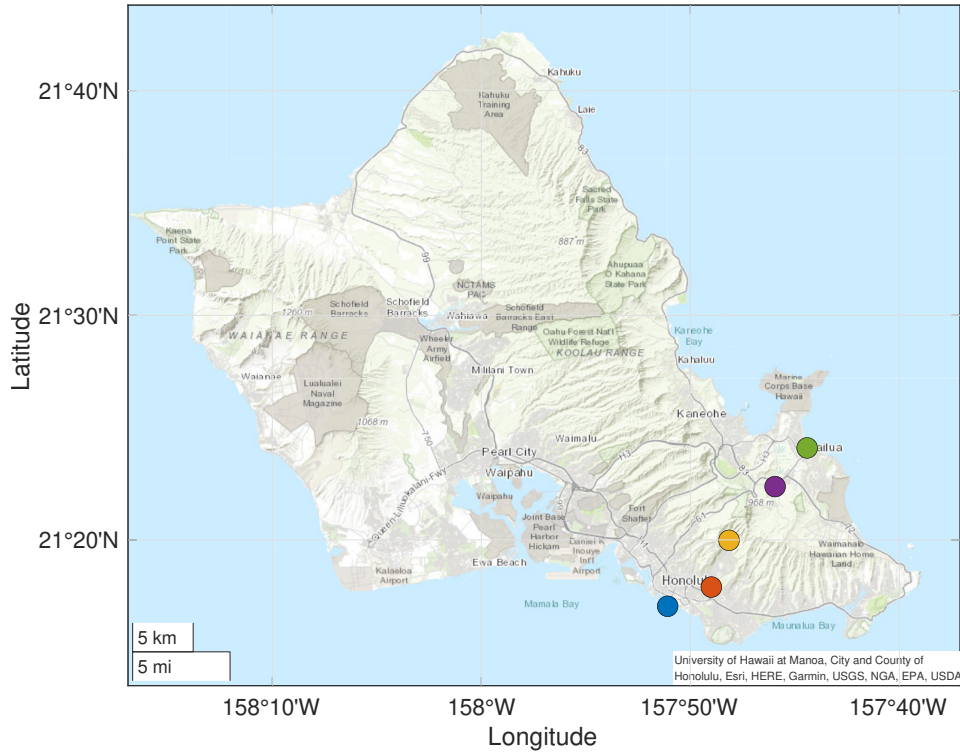


Figure 1. Topographic map of O'ahu with the five sites marked by colored circles: Kailua (green), Maunawili (purple), Lyon Arboretum (yellow), HIG (orange), and Waikikī (blue).

Table 1. Summary of information relative to the sites deployed on O'ahu to collect the data used in this manuscript.

Site	Latitude	Longitude	Elevation	Deployment	Samples
Kailua	21° 24 '60" N	-157° 44' 25" E	8.5 m	07/06/2019 - current	110
Maunawili	21° 22' 22" N	-157° 45' 57" E	27.4 m	10/05/2019 - current	68
Lyon Arb.	21° 19' 59" N	-157° 48' 09" E	132.3 m	07/25/2019 - current	104
HIG	21° 17' 54" N	-157° 48' 60" E	40.8 m	09/28/2019 - current	81
Waikikī	21° 17' 02" N	-157° 50' 29" E	2 m	10/04/2019 - 03/14/2020	13

196 Because the data was collected a little over two years, data from the Global Net-
 197 work of Isotopes in Precipitation (GNIP) are also considered to investigate interannual
 198 variability of rainfall isotopic composition in Hawai'i. GNIP is a network that was cre-
 199 ated in 1957 by the International Atomic Energy Agency and the World Meteorologi-
 200 cal Organization (IAEA/WMO, 2021). Sites were deployed in multiple locations through-
 201 out the entire world, and collections were typically done with a monthly frequency. In
 202 Hawai'i, only one GNIP site was deployed in Hilo, a town on the windward side of Hawai'i
 203 Island, and data were collected from 1962 until 1970.

204 **2.3.2 Isotope analysis**

205 Hydrogen and oxygen isotopic composition of rainwater was determined using cav-
 206 ity ring-down spectroscopy (a L2130-I, Picarro) equipped with a high-precision vapor-
 207 izer (V1102-I, Picarro, Inc., Santa Clara, CA, USA) and autosampler (HTC PAL, Leap
 208 Technologies, Carrboro, NC, USA) with Chem-Correct acquisition software that mon-
 209 itors for interference of isotopologues of water by organic compounds (Gupta et al., 2009).
 210 All measurements were performed in the nitrogen carrier mode, using ultra-high-purity
 211 nitrogen (< 10 ppm H_2O , $> 99.99\%$ N_2 ; ALPHAGAZ1, Air Liquide, Houston, TX, USA).
 212 Samples were normalized to VSMOW using results of analysis of at least three labora-
 213 tory reference materials that were extensively calibrated with NIST reference materials
 214 and had $\delta^2\text{H}$ and $\delta^{18}\text{O}$ values that bracketed the values of all samples. These laboratory
 215 reference waters were analyzed so that they bookended every 8 to 14 unknowns. Based
 216 on repeated measurements of an internal laboratory reference water similarly calibrated
 217 using NIST reference material and analyzed as an unknown, the precision for this method
 218 was less than $\pm 0.05\%$ for $\delta^{18}\text{O}$ values and $\pm 0.5\%$ for $\delta^2\text{H}$ values.

219 **2.3.3 Weather data at Lyon Arboretum and HIG**

220 Hourly rainfall data from HIG were collected using a Campbell Scientific TE525WS
 221 Texas Electronics Tipping Gauge (8" orifice), whereas hourly relative humidity data were
 222 collected using a Campbell Scientific EE181-L Air Temperature and Relative Humidity
 223 sensor. The former has accuracy of $\pm 1\%$ at rates up to 1 inch/hour, whereas the latter
 224 has accuracy of $\pm 1.3\%$ for temperatures and relative humidities typically found on O'ahu.
 225 The data cover a time interval between 16 October 2019 and 27 August 2021.

226 Rainfall and relative humidity data from Lyon Arboretum were collected at a 15-
 227 minute frequency using a CR3000 Campbell Scientific data logger and associated sen-
 228 sors (HUMICAP 180R sensor for relative humidity). In order for rainfall data to be di-
 229 rectly comparable with those from HIG, they were converted into hourly with a simple
 230 accumulation sum. For typical conditions at Lyon Arboretum, the accuracy of the hu-
 231 midity sensor is $\pm 1\%$, whereas for the rain gauge it is $\pm 1\%$ up to 2 inches/hour of rain.
 232 Both rainfall and relative humidity data at Lyon Arboretum cover a period from 23 Febru-
 233 ary 2018 until 26 April 2021.

234 When comparing datasets from HIG and Lyon Arboretum, an intersection of the
 235 two distinct temporal windows (16 October 2019 - 26 April 2021) is considered to select
 236 the data.

237 **2.3.4 HYSPLIT**

238 In order to diagnose the origin of air parcels flowing over O'ahu, the NOAA Air
 239 Resources Laboratory's Hybrid Single Particle Lagrangian Integrated Trajectory (HYS-
 240 PLIT) model, version 5.1.0 for Linux, was used (Draxler & Hess, 1998; Stein et al., 2015).
 241 The model uses meteorological data to compute the forward/backward transport and
 242 dispersion of a tracer or of a number of trajectories. It is extensively used in the study

243 of atmospheric processes, with applications including transport of pollutants, allergens,
244 or volcanic ash (Stein et al., 2015).

245 Following similar approaches (Sodemann et al., 2008; Barras & Simmonds, 2009;
246 Guan et al., 2013; Aemisegger et al., 2014; Papritz et al., 2021; Villiger et al., 2021; Dahin-
247 den et al., 2021), HYSPLIT was used to interpret the deuterium excess data. First, a
248 temporal window of 24 months, from 01 July 2019 until 30 June 2021 was selected. This
249 choice was made in order to maximize the overlap with the collected isotope data and
250 also to maintain a symmetry between the number of wet- and dry-season months con-
251 sidered. Then, for each day during the time window, 27 trajectories were initialized at
252 a point with the same latitude-longitude coordinates as Lyon Arboretum at an altitude
253 of 500 m, and their positions were integrated backward in time for 5 days. The integra-
254 tion was conducted using meteorological data from ERA5 reanalysis (Hersbach et al.,
255 2019).

256 The choice of initializing the trajectories at 500 m was made to ensure that the cal-
257 culation would capture air parcels that are most likely to contribute to rainfall on O‘ahu:
258 because of the trade-wind inversion that persists at an altitude of approximately 2-2.5
259 km for most of the year (Cao et al., 2007), parcels in the free troposphere are unlikely
260 to contribute often, except during precipitation from synoptic systems. Sensitivity tests
261 were conducted by initializing trajectories at 2,500 m and at 5,000 m, but the conclu-
262 sions reached were qualitatively the same. Sensitivity tests were also conducted by only
263 considering trajectories initialized in periods when rainfall was collected at Lyon Arbore-
264 tum, but no qualitative difference was noticed.

265 **3 Results**

266 **3.1 Rainfall**

267 For the collection period discussed here, the time series of rainfall rates observed
268 at each site are presented in Figure 2a. The rates are computed by dividing the amount
269 of water collected at each sampling period by the number of days over which the collec-
270 tion took place (Giambelluca et al., 2013). As expected, the figure shows that the high-
271 est rain rates were recorded during the wet season, between the months of October and
272 April. These peaks are typically due to Kona lows, like those in March 2020 and 2021,
273 or cold fronts affecting the islands, responsible for the peaks observed in mid-to-late De-
274 cember and January 2019, or the local maximum observed in early February 2021, which
275 led to the formation of a number of deep convective storms on O‘ahu.

276 The dry season tends to be characterized by lower rain rates, mostly due to trade
277 wind showers. Occasionally, TCs and tropical storms (TSs) can affect the Hawaiian Is-
278 lands during the dry season. During the collection period, 4 TC/TS events were recorded.
279 First, on 8 July 2019, the remnants of TC Barbara passed south of the islands and brought
280 rainfall to the islands, especially on the windward side. Following that, the remnants of
281 TC Erik and Flossie also affected Hawai‘i on 12 and 16 July 2019, respectively. Although,
282 as will be seen later, rainfall from these three systems had a different isotopic compo-
283 sition compared to trade-wind showers, the rainfall rates were not significantly higher.
284 The following year, TC Douglas passed remarkably close to the Hawaiian Islands around
285 25 July 2020. Enhanced rainfall rates by Douglas can be seen in Figure 2a, especially
286 for the Kailua and the Lyon Arboretum site.

287 Another important feature shown by Figure 2a is that significantly more rainfall
288 is often collected at Lyon Arboretum than all the other sites. For example, as can be in-
289 ferred from Figure 2b, the median rain rate at Lyon Arboretum is 8.03 mm day^{-1} , whereas
290 at HIG, only 4 km downwind, it is 1.35 mm day^{-1} , which is comparable to the median
291 rate recorded at the other sites. Considering the location of the Lyon Arboretum

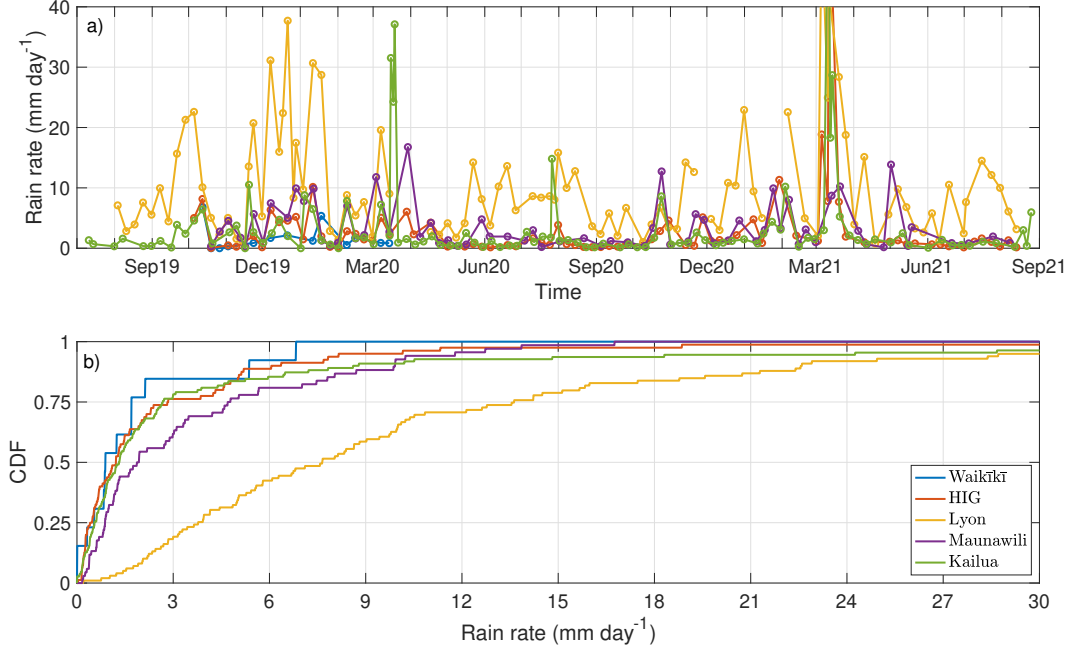


Figure 2. a) Time series of rain rates for the five sites, determined as the total accumulated rain for each collection period divided by the time since the previous collection. b) Cumulative distribution functions of rain rates.

292 rain collector, this can easily be explained as due to orographic enhancement provided
 293 by the Ko‘olau mountains.

294 3.2 Rainfall ^2H and ^{18}O isotopic composition

295 The time series of $\delta^2\text{H}$ and $\delta^{18}\text{O}$ values for the five deployed sites are shown in Fig-
 296 ure 3a and 3b, respectively. Precipitation from two Kona lows (March 2020 and 2021)
 297 has the lowest $\delta^{18}\text{O}$ and values of all the collection period, with particularly low $\delta^2\text{H}$ val-
 298 ues ($\sim 64.0\%$) recorded at the Kailua station. Rainfall from TCS, or their remnants,
 299 also appear to have low $\delta^2\text{H}$ and $\delta^{18}\text{O}$ values, although not as low as Kona lows ($\delta^2\text{H} \sim$
 300 -32.0%). A low pressure system to the north of the islands on 10-11 October 2019 led
 301 to the advection of moist flow from the southeast, which ultimately resulted in a series
 302 of thunderstorms that produced very low $\delta^2\text{H}$ values ($\sim -52.6\%$ at the Waikiki site).
 303 Thunderstorms were also observed during other periods, for example on 18-19 Novem-
 304 ber 2019 and on 3 February 2021, but the rainfall they produced did not have partic-
 305 ularly low values of $\delta^2\text{H}$ and $\delta^{18}\text{O}$.

306 Figure 4a shows the times series of $\delta^{18}\text{O}$ values of rainfall as a function of the av-
 307 erage rain rate during each collection period ($\delta^2\text{H}$ values look very similar but is not shown).
 308 Because Lyon Arboretum is characterized by larger rain rates than any other site, and
 309 given that the sites have similar distribution functions of rain rates (Figure 2b), the data
 310 are presented as a function of rain rate percentiles. Rainfall, particularly during the dry
 311 season (Figure 4c), appears to have a remarkably consistent isotopic composition, although,
 312 as Figure 2b illustrates, the bottom 75 percentiles correspond to relatively small rain rates,
 313 especially for leeward sites. Nevertheless, for those rain rates, rainfall collected at HIG
 314 tends to be enriched in ^{18}O by 1-1.5 ‰ than at any other site.

315 In order to gain a more quantitative understanding of the isotopic composition of
 316 rainfall collected, and in order to compare the data with similar datasets on O‘ahu, a

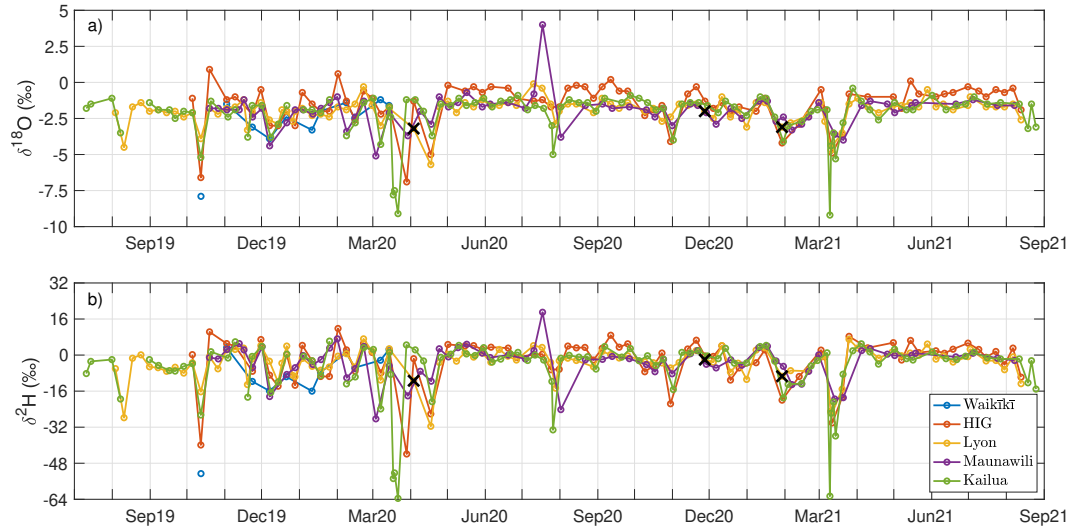


Figure 3. Time series of $\delta^{18}\text{O}$ (a) and $\delta^2\text{H}$ (b) values for the five sites: Kailua (green); Maunawili (purple); Lyon Arboretum (yellow); HIG (orange); Waikīkī (blue). Black crosses represent data collected when the sampler had overflowed.

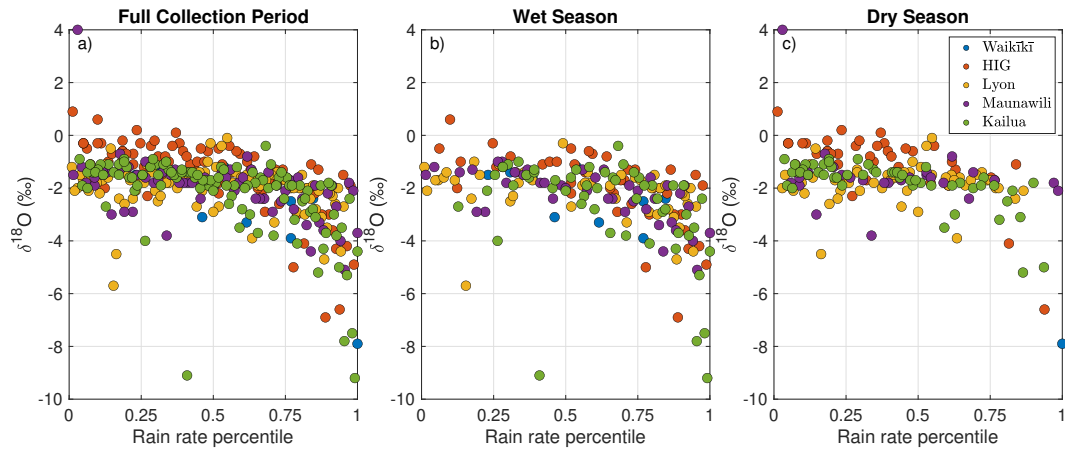


Figure 4. $\delta^{18}\text{O}$ values as a function of rain rate percentile for each site shown for the entire collection period (a), only considering wet-season rainfall (b), and only considering dry-season rain (c).

Table 2. Volume-weighted averages of $\delta^{18}\text{O}$ and $\delta^2\text{H}$ values and deuterium excess for the five sites computed considering all the collection period (1st, 4th, and 7th rows), only the wet seasons (2nd, 5th, and 8th rows), and only the dry season (3rd, 6th, and 9th rows). Numbers in parentheses represent standard errors associated with the mean values.

	Waikīkī	HIG	Lyon Arb.	Maunawili	Kailua
$\delta^2\text{H}_{tot}(\text{‰})$	-19.39 (5.81)	-11.56 (1.57)	-3.99 (0.67)	-7.99 (1.10)	-14.57 (1.83)
$\delta^2\text{H}_{wet}(\text{‰})$	-8.93 (1.78)	-12.44 (2.10)	-4.89 (1.13)	-10.30 (1.44)	-18.16 (2.84)
$\delta^2\text{H}_{dry}(\text{‰})$	-52.60	-8.51 (2.49)	-2.92 (0.63)	-1.67 (0.86)	-6.53 (1.26)
$\delta^{18}\text{O}_{tot}(\text{‰})$	-3.79 (0.73)	-2.85 (0.20)	-2.10 (0.09)	-2.63 (0.13)	-3.32 (0.21)
$\delta^{18}\text{O}_{wet}(\text{‰})$	-2.50 (0.27)	-3.02 (0.26)	-2.38 (0.13)	-2.94 (0.16)	-3.77 (0.33)
$\delta^{18}\text{O}_{dry}(\text{‰})$	-7.90	-2.26 (0.35)	-1.75 (0.09)	-1.77 (0.11)	-2.30 (0.16)
$d_{tot}(\text{‰})$	10.93 (0.73)	11.23 (0.29)	12.78 (0.32)	13.04 (0.32)	11.97 (0.30)
$d_{wet}(\text{‰})$	11.04 (0.87)	11.71 (0.37)	14.18 (0.46)	13.25 (0.40)	12.01 (0.46)
$d_{dry}(\text{‰})$	10.60	9.61 (0.42)	11.11 (0.33)	12.46 (0.52)	11.88 (0.28)

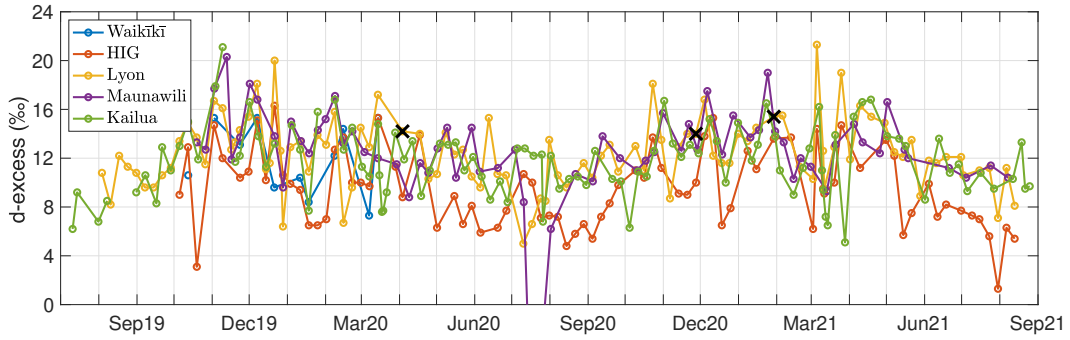


Figure 5. Time series of deuterium excess for each site during the entire collection period, from July 2019 to August 2021. The colors of the time series are the same as Figure 3. Black crosses represent data collected when the sampler had overflowed.

317 summary of the volume-weighted averages of isotopic abundances for each site is given
 318 in Table 2.

319 3.3 Deuterium excess

320 The time series of deuterium excess derived from Equation 4 for the five sites is pre-
 321 sented in Figure 5. The figure presents two interesting features. The first is the appar-
 322 ent seasonal cycle, with higher deuterium excess during the wet season and lower val-
 323 ues during the dry season, and a difference between the two of approximately 5 ‰. This
 324 phenomenon has been observed both on a global scale (Araguás-Araguás et al., 2000;
 325 Pfahl & Sodemann, 2014) and at a regional level in other locations (Delmotte et al., 2000;
 326 Yoshimura & Ichianagi, 2009; Guan et al., 2013; Kopec et al., 2019). Because deuterium
 327 excess has been shown to be sensitive to relative humidity and SST at the moisture source
 328 (Merlivat & Jouzel, 1979; Uemura et al., 2008; Pfahl & Sodemann, 2014), changes in the
 329 environmental conditions at the source, or the presence of difference sources, are typ-

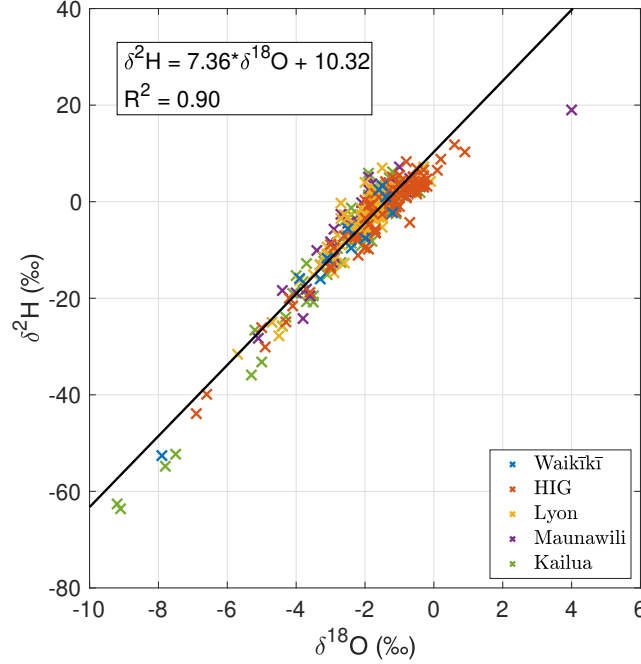


Figure 6. LMWL (black line) diagnosed from a linear regression of all the data from the five sites (colored crosses) over the entire collection period. The slope and the intercept of the linear regression, as well as the R^2 are reported in the top-left corner.

330 ically used to explain seasonal changes to deuterium excess values. Another interesting
 331 feature in Figure 5 is that, particularly during the dry season, the HIG site has consis-
 332 tently lower deuterium excess compared to other sites. A more quantitative comparison
 333 of the deuterium excess values measured at the five sites is presented in the last three
 334 rows of Table 2, which represent the volume-weighted averages for the entire collection
 335 period, for the wet season and for the dry season only.

336 3.4 The Local Meteoric Water Line

337 The black line in Figure 6 represents the LMWL for O‘ahu determined using a lin-
 338 ear regression based on all the data collected (shown in colored crosses). While most data
 339 points seem to align relatively well with the LMWL, data at the extremes—either very
 340 low or very high values of $\delta^2\text{H}$ and $\delta^{18}\text{O}$ —appear to lie under the LMWL, potentially an
 341 indication of sub-cloud rain evaporation. The slope and the intercept of the LMWL are
 342 reported in Table 3.

343 As a way to test the sensitivity of the LMWL to the geography of the network and
 344 the temporal window over which the collection is conducted, Table 3 also reports results
 345 from a simple experiment. The second and third row are obtained by first subdividing
 346 the sites into those on the windward side of the island (Kailua and Maunawili) and those
 347 on the leeward side (Lyon Arboretum, HIG, and Waikīkī). The fourth and the last row
 348 contain results from regressions conducted using all data from 01 July 2019 until 30 June
 349 2020, and from 01 July 2020 until 30 June 2021, respectively. The results show consid-
 350 erable variability, which naturally raises the question of what spatial and temporal scales
 351 must be taken into consideration in order to determine a LMWL which is representa-
 352 tive of O‘ahu and, more generally, the Hawaiian Archipelago.

Table 3. Slopes and intercepts of LMWL computed using the entire dataset (1st row), considering only the sites on the windward side (2nd row), those on the leeward side (3rd row), or only data during the first or the second collection year (4th and 5th rows, respectively). The last row contains the slope and the intercept of the LMWL determined by Dores et al. (2020). Numbers in parentheses represent standard deviations.

	Slope (‰/‰)	Intercept (‰)
Total	7.36 (0.13)	10.32 (0.30)
Windward	7.70 (0.18)	11.44 (0.46)
Leeward	7.02 (0.18)	9.34 (0.40)
Year 1	7.77 (0.16)	11.49 (0.42)
Year 2	6.89 (0.20)	9.21 (0.43)
Dores et al. (2020)	7.22	10.31

4 Discussion

Although the hydrogen and oxygen isotopic composition of water has been used in many different areas within the study of climate, an incomplete understanding of how various atmospheric processes affect the isotopic composition of precipitation contributes to making the interpretation of records difficult. While numerical models can be a key to progress, the relative lack of long-term high-frequency time series of $\delta^2\text{H}$ and $\delta^{18}\text{O}$ values can be a hindrance to this progress. This study contributes to the current debate by introducing a new dataset of rainfall isotopic composition on the Island of O‘ahu. Compared to other collections conducted in the Hawaiian Islands in the past decades, this dataset has a much higher temporal resolution and, at the same time, it also includes multiple sites spread across a mountainous range on the island.

4.1 Rainfall isotopic composition

Even though they were collected at different frequencies and over different time periods, the data presented in this work compare favorably with those discussed in Dores et al. (2020). In particular, in almost all sites, rainfall appears to be characterized by lower values of $\delta^2\text{H}$ and $\delta^{18}\text{O}$ during the wet season than the dry season, something that had been noticed by collections on the other islands as well (Scholl et al., 1996, 2002, 2007; Tillman et al., 2014; Kelly & Glenn, 2015; Fackrell et al., 2020; Tachera et al., 2021). One advantage of the data discussed here, however, is that the increased temporal resolution gives a clearer picture of the isotopic composition of rainfall due to different types of synoptic systems or weather disturbances. For example, Figure 3 revealed that Kona lows, subtropical storms that happen during the wet season can generate precipitation with, for example, $\delta^2\text{H}$ values as low as -64‰ . Other precipitating systems, like cold fronts or thunderstorms were also associated with low $\delta^2\text{H}$ and $\delta^{18}\text{O}$ values, but not as much as Kona lows. The differences in the rainfall isotopic composition of various weather systems and their seasonality might also explain why wet-season isotopic compositions appear to be characterized by greater variability than dry-season ones (Figures 3a and b).

A series of recent works presented reconstructions of precipitation $\delta^2\text{H}$ values obtained from peatlands on Moloka‘i (Beilman et al., 2019) and O‘ahu (Massa et al., 2021) over the last 12 ka and 45 ka before present (BP), respectively. The data show periods characterized by low $\delta^2\text{H}$ values of peatland water—e.g., 3 ka and 9-10 BP—interspersed

384 by longer periods of comparatively higher values. The authors interpreted the low val-
 385 ues as suggestive of an increased activity of Kona lows and cold fronts during those time
 386 intervals. Apart from providing support to this interpretation, the dataset presented in
 387 this manuscript also suggests that rainfall from Kona lows presents lower $\delta^2\text{H}$ values than
 388 that from cold fronts. Taken together, these results could imply that low $\delta^2\text{H}$ values in
 389 peatland water might be a reflection of changes in Kona low activity, as changes in cold
 390 front and extratropical storm activity would be unlikely to leave a strong isotopic sig-
 391 nature in the paleorecord. On such long time scales, however, other factors might also
 392 play a role: for example, changes in vegetation cover might lead to greater evapotran-
 393 spiration rates, which could affect the rainfall isotopic composition (Scholl et al., 2007).
 394 A detailed analysis of this is beyond the scope of this manuscript and is left for future
 395 work.

396 The dataset presented in this manuscript also allows an assessment of the spatial
 397 variability of rainfall $\delta^2\text{H}$ and $\delta^{18}\text{O}$ values. Considering that the climate in the Hawai-
 398 ian Islands is dominated by trade winds, which blow with an easterly/northeasterly di-
 399 rection, a reasonable a priori expectation would be that rainfall collected on the wind-
 400 ward side of the island is more enriched in ^2H and ^{18}O than that on the leeward side:
 401 as the air flow is lifted by the island orography, water vapor first condenses and then pre-
 402 cipitation forms; as clouds continue their journey across the island, progressive rainout
 403 leads to lower $\delta^2\text{H}$ and $\delta^{18}\text{O}$ values in rainfall. The data presented here, however, paint
 404 a more complex picture.

405 While Figure 3 and Table 2 suggest that ^2H and ^{18}O abundances at the Waikīkī
 406 site are generally lower than at the Kailua site, particularly during the dry season, $\delta^2\text{H}$
 407 and $\delta^{18}\text{O}$ values seem to progressively increase as the air flows over the Ko‘olau Range
 408 and then decrease again as it flows past the mountains. As Figure 2b shows, the sites
 409 at Maunawili and Lyon tend to have higher precipitation rates than other sites (Giambelluca
 410 et al., 2013), so that one might expect $\delta^2\text{H}$ and $\delta^{18}\text{O}$ values to be lower there (Dansgaard,
 411 1964).

412 One hypothesis to explain this apparent paradox, at least in part, is that different
 413 weather systems affect the five sites in different ways, due to their different windward
 414 and leeward locations across the Ko‘olau Mountain Range, and they do not necessar-
 415 ily bring rainfall in proportional amounts to the five sites. For example, cold fronts and
 416 Kona lows, which are associated with low values of $\delta^2\text{H}$ and $\delta^{18}\text{O}$, have a size and an in-
 417 tensity that likely affects the entire island of O‘ahu, or at least substantial portions of
 418 it. On the other hand, trade-wind showers, which tend to have comparatively higher val-
 419 ues of $\delta^2\text{H}$ and $\delta^{18}\text{O}$ than Kona low rainfall, are largely caused by the orographic lift-
 420 ing provided by the Ko‘olau mountains. Because of the easterly/northeasterly direction
 421 of the winds, trade-wind showers are likely to lead to large amounts of rain on the sum-
 422 mits and immediately downwind of the mountains, where Lyon Arboretum is located.
 423 However, since the orographic forcing ceases after passing the mountain summits, many
 424 of these showers stop before reaching the HIG site. Thus, trade-wind showers affect Lyon
 425 Arboretum disproportionately compared to the rest of the network and cause the volume-
 426 weighted average to be higher than other places.

427 To check the consistency of this hypothesis, the daily accumulated rainfall at HIG
 428 is matched with the daily accumulated rainfall at Lyon Arboretum, and the result is pre-
 429 sented in Figure 7a. If HIG is receiving only proportionately less rainfall for each event
 430 affecting Lyon Arboretum, one would expect a good correlation between the daily ac-
 431 cumulated rainfall at both sites. Instead, rainfall appears not particularly correlated, and
 432 there seem to be many days when rainfall is recorded at Lyon Arboretum but not at HIG,
 433 particularly during the dry season, where rainfall is mostly due to trade-wind showers.

434 Figure 7b shows the cumulative distribution function of daily accumulated rain-
 435 fall at HIG for days when more than 0.5 mm of rain was collected at Lyon Arboretum.

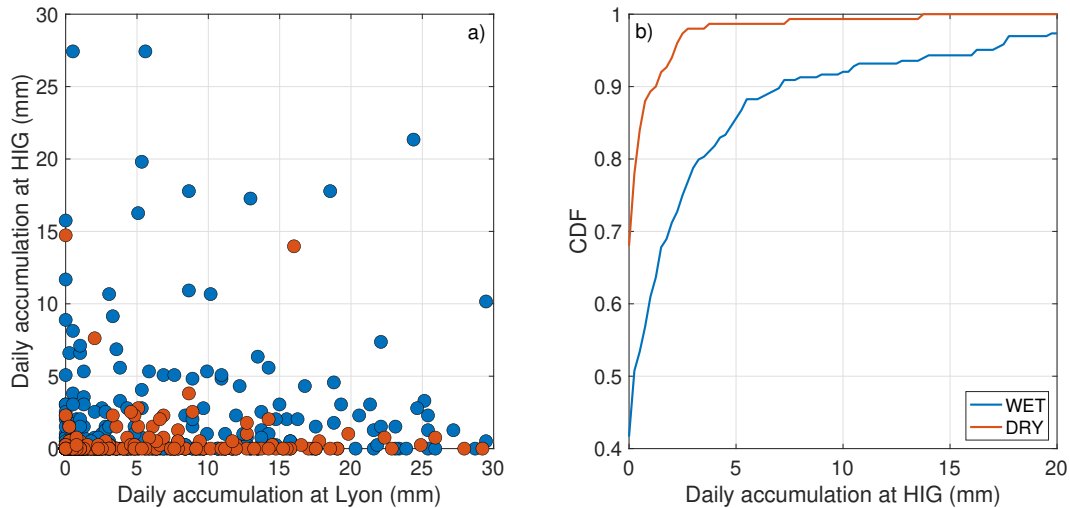


Figure 7. a) Daily accumulated rainfall at HIG shown as a function of rainfall accumulated at Lyon Arboretum for the same day. b) Cumulative distribution function of daily accumulated rainfall at HIG for days during the wet (blue) and dry (red) season when more than 0.5 mm of rain was collected at Lyon Arboretum.

436 The curves show that, for 41.5% of those days during the wet season and for 68.0% during
 437 the dry season, no rainfall was collected at HIG in spite of some being recorded at
 438 Lyon Arboretum. The numbers increase when attention is restricted to days with small
 439 amounts of precipitation at Lyon Arboretum that do not exceed 5 mm (53.3% during
 440 the wet season and 72.6% during the dry season; not shown).

441 Differences in precipitation frequency due to the orographic effect might partially
 442 explain the values of ^2H and ^{18}O isotope abundances observed in Table 2, although other
 443 factors could also contribute. For example, Figures 3 and 4 suggest that in many events,
 444 particularly during dry seasons, rainfall at the HIG site had higher $\delta^2\text{H}$ and $\delta^{18}\text{O}$ val-
 445 ues than other stations. Furthermore, Figure 5 shows that, for those events, rainfall at
 446 HIG also has lower deuterium excess than other stations. It is hypothesized that these
 447 differences can be explained in terms of rain evaporation. Figure 8 represents the diurnal
 448 cycle of the average relative humidity at Lyon Arboretum (yellow) and HIG (purple).
 449 The figure shows a differences between the relative humidity at Lyon Arboretum
 450 and HIG of the order of 10%, which supports the hypothesis that rain collected at the
 451 latter site experiences significant amounts of rain evaporation. This is perhaps not sur-
 452 prising considering that Lyon Arboretum is at the back of the Mānoa Valley and is sur-
 453 rounded by vegetation, whereas HIG is in a more urban setting. The sharp gradient of
 454 relative humidity in a relatively short space is an illustration of strong variability of mi-
 455 croclimates on the Hawaiian Islands. During rain evaporation, kinetic fractionation leads
 456 to an enrichment of rainfall ^2H and ^{18}O isotopes and to lower values of deuterium ex-
 457 cess.

458 A close examination of the data also suggests that rainfall $\delta^2\text{H}$ and $\delta^{18}\text{O}$ values are
 459 higher at the Maunawili site, on the windward side but close to the Koʻolau Range, than
 460 at Kailua, also on the windward side but farther away from the mountains and closer
 461 to the ocean. Deuterium excess is also higher in precipitation in Maunawili than in Kailua.
 462 As argued by Scholl et al. (2007) when interpreting differences between windward and
 463 leeward rainfall isotopic composition on Maui, it is possible that a higher abundances
 464 and higher deuterium excess might indicate that air flowing over the island entrains wa-
 465 ter vapor that has been evapotranspired from the local vegetation (a processed they re-

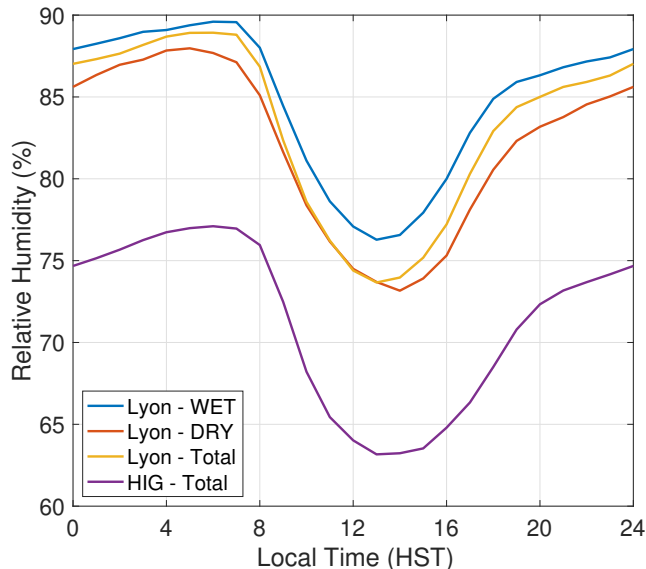


Figure 8. Average diurnal cycles of relative humidity at Lyon Arboretum for the entire period (yellow), for the wet (blue) and the dry (red) season only, and at HIG for the entire period (purple).

466 referred to as "recycling"). Unfortunately, using rainfall ^2H and ^{18}O abundances alone,
 467 it is hard to draw any definitive conclusion. A follow-up paper is in preparation in which
 468 isotope-enabled cloud resolving models are used precisely to address these types of ques-
 469 tions.

470 Another important point that emerges from the systematic differences observed in
 471 the dataset, as well as with other extended network of sites in Hawai'i (Scholl et al., 2007;
 472 Does et al., 2020), is that caution should be taken when using data from single sites in
 473 locations with complex topography. In the case of Hawai'i, for example, GNIP collected
 474 many years of data in a single location in Hilo, on the windward side of Hawai'i Island.
 475 If indeed, as suggested by Scholl et al. (2007) for Maui, windward locations experience
 476 stronger water vapor recycling in the presence of significant topography, isotope data in
 477 Hilo might have systematically lower $\delta^2\text{H}$ and $\delta^{18}\text{O}$ values and higher deuterium excess
 478 than rainfall over the open ocean.

479 4.2 Deuterium excess and moisture origin

480 As briefly discussed in Section 3.3, the deuterium excess values shown in Figure
 481 5 present seasonal variations at all the sites. Consistent with other observations across
 482 the planet (Araguás-Araguás et al., 2000; Delmotte et al., 2000; Yoshimura & Ichiyanagi,
 483 2009; Guan et al., 2013; Pfahl & Sodemann, 2014; Kopec et al., 2019), this behaviour
 484 for data in Hawai'i is hypothesized to be due to changes in the air masses that contribute
 485 to precipitation at different times of the year: while synoptic systems that are respon-
 486 sible for much of the rainfall during the wet season originate in the Northwestern Pa-
 487 cific (K. Kodama & Barnes, 1997; K. R. Kodama & Businger, 1998), rainfall during the
 488 dry season is mostly due to the trade-wind flow, which originates in the Northeastern
 489 part of the Pacific basin.

490 In order to assess the consistency of this hypothesis, the backward trajectories gener-
 491 ated with HYSPLIT (see Section 2.3.4) are considered. First, the trajectories are di-
 492 vided in those initiated during the wet season and those during the dry season. Then,

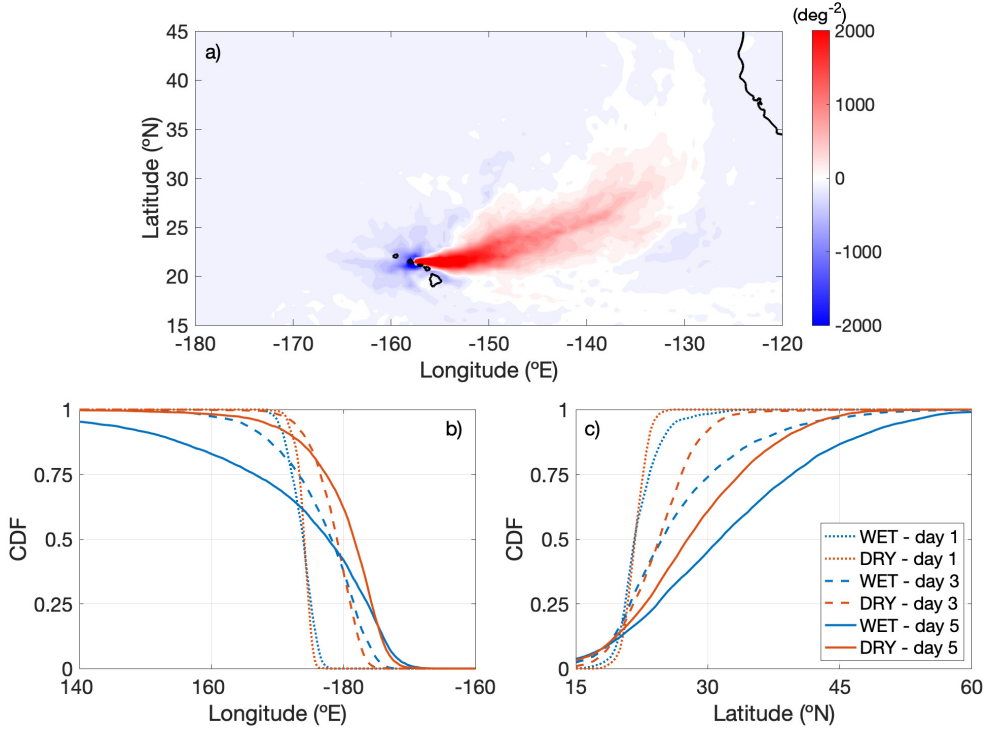


Figure 9. a) Differences in trajectory densities between dry- and wet-season months; Cumulative distribution function of longitude (b) and latitude (c) coordinates for trajectories during the wet (blue) and dry (red) season at 1 (dotted), 3 (dashed), and 5 (continuous) days prior to their initialization.

493 histograms are derived based on the latitude and longitude of each trajectory at any point
 494 in its history. The difference between the histogram for the dry season and that for the
 495 wet season is shown in Figure 9a. The plot shows that, during the dry season, trajec-
 496 tories tend to have a more coherent north-eastern origin, which is consistent with trade
 497 winds being more prevalent during this time of year. During the wet season, many tra-
 498 jectories still originate from the high-pressure area to the north-east of O‘ahu, although
 499 a considerable number of trajectories originate to the west and to the north of the is-
 500 land.

501 In order to quantify these differences, the cumulative distribution function of partic-
 502 les’ longitudes at different times during the wet season (blue) and the dry season (red)
 503 is shown in Figure 9b. The figure suggests that, five days ahead of the particles’ initi-
 504 ation time, there is a difference of 21.5° in longitude of the 75th percentile of the dis-
 505 tribution for the wet and the dry season trajectories. Figure 9c shows a difference of 6°
 506 for the 75th percentiles of wet and dry season trajectories.

507 Considering the differences between SST and relative humidity in the Central and
 508 West Pacific during the winter months and those in the Eastern Pacific during the sum-
 509 mer months (see, e.g., Figure 2 of Pfahl and Sodemann (2014)), the analysis above sup-
 510 ports the hypothesis that differences in the moisture sources contributing to the precip-
 511 itating events of the wet and dry season could help explain the seasonal changes in deu-
 512 terium excess observed.

513 This suggests a connection between the deuterium excess found in rainfall in Hawai‘i
 514 and the large-scale dynamics that influence the climate in the North Pacific region. In

principle, this connection could be used to diagnose, or at least provide further constraints on those dynamics at times for which there was insufficient coverage of meteorological data, for example when the GNIP site in Hilo was active, or in the interpretation of paleoclimate data, assuming that both $\delta^{18}\text{O}$ and $\delta^2\text{H}$ values are available.

On a more local scale, another potential contributing factor that would lead to seasonal changes of deuterium excess are differences in rain evaporation that precipitating columns experience in different seasons. The blue and red curves in Figure 8 the diurnal cycle of the average relative humidity at Lyon Arboretum during the wet and the dry season, respectively. In spite of the similarities between the two curves, relative humidity values during the dry season are lower than the wet-season curve by 4-5%. This is particularly evident in the afternoon/evening, when a peak in rainfall from trade-wind showers is often observed in many locations across the island (Hartley & Chen, 2010). Assuming that the spectrum of raindrops does not vary too much throughout the year, rain that falls during the dry season should experience more rain evaporation.

4.3 Interannual variability

In Section 3.4, the LMWL computed from the network of sites was presented. Even though the network used here covers a much smaller area than the network used by Dores et al. (2020), the LMWLs are comparable. However, as also highlighted by Dores et al. (2020), considering all the isotope collections that have been made in Hawai'i, some important differences emerge. For example, from a 2-year collection conducted on East Maui, Scholl et al. (2002) computed a LMWL with slope and intercept of 8.2 ‰/‰ and 14.7 ‰ respectively, significantly different values compared to those reported here. Similarly, Fackrell et al. (2020) used a 2-year collection on West Hawai'i to determine a LMWL with a slope of 7.65 ‰/‰ and an intercept of 15.25 ‰. While the former is comparable to what was reported in Table 3, the latter is significantly higher. One might argue that different parts of different islands experience different climatic conditions, such as evapotranspiration, temperature, and relative humidity, and these differences are reflected in the LMWLs. However, Tachera et al. (2021) recently determined a LMWL for a similar area to that considered by Fackrell et al. (2020) and found a significantly higher slope (8.14 ‰/‰) and a lower intercept (12.83 ‰).

Discussing seasonal variations of deuterium excess naturally leads one to wonder what is the interannual variability of $\delta^{18}\text{O}$ and $\delta^2\text{H}$ values in Hawai'i. In their analysis of rainwater isotopic composition collected on Hawai'i Island, Tachera et al. (2021) determined a different LMWL than that Fackrell et al. (2020) had produced from data collected in the same area only a few years before. A linear interpolation of the isotopic data in this manuscript gave a LMWL that was comparable to the one computed by Dores et al. (2020) on the island of O'ahu, but, on the other hand, Table 3 illustrates how subsampling data could give rise to LMWLs with very different characteristics.

In order to gain a better appreciation of the intraseasonal variability of the rainfall isotopic composition in Hawai'i, Figure 10a and 10b represent the isotopic abundances recorded at the GNIP site of Hilo during the wet and the dry season, respectively. The plots show that, while rain during the dry season tends to have a more consistent isotopic composition throughout the years of data collection, rain during the wet season shows significant differences: although with some exceptions, years in the second part of the collection tend to have lower $\delta^{18}\text{O}$ and $\delta^2\text{H}$ values than those in the first part. Figures 10c and 10d show deuterium excess as a function of $\delta^{18}\text{O}$ values during the wet and dry season, respectively. Rainfall with lower $\delta^{18}\text{O}$ and $\delta^2\text{H}$ values appears to have slightly higher deuterium excess than that with higher $\delta^{18}\text{O}$ and $\delta^2\text{H}$ values.

These figures suggest a significant interannual variability of rainfall isotopic composition during the wet season, and only a modest variability for dry-season precipitation. In turn, based on the prior discussion, the variability during wet-season months is

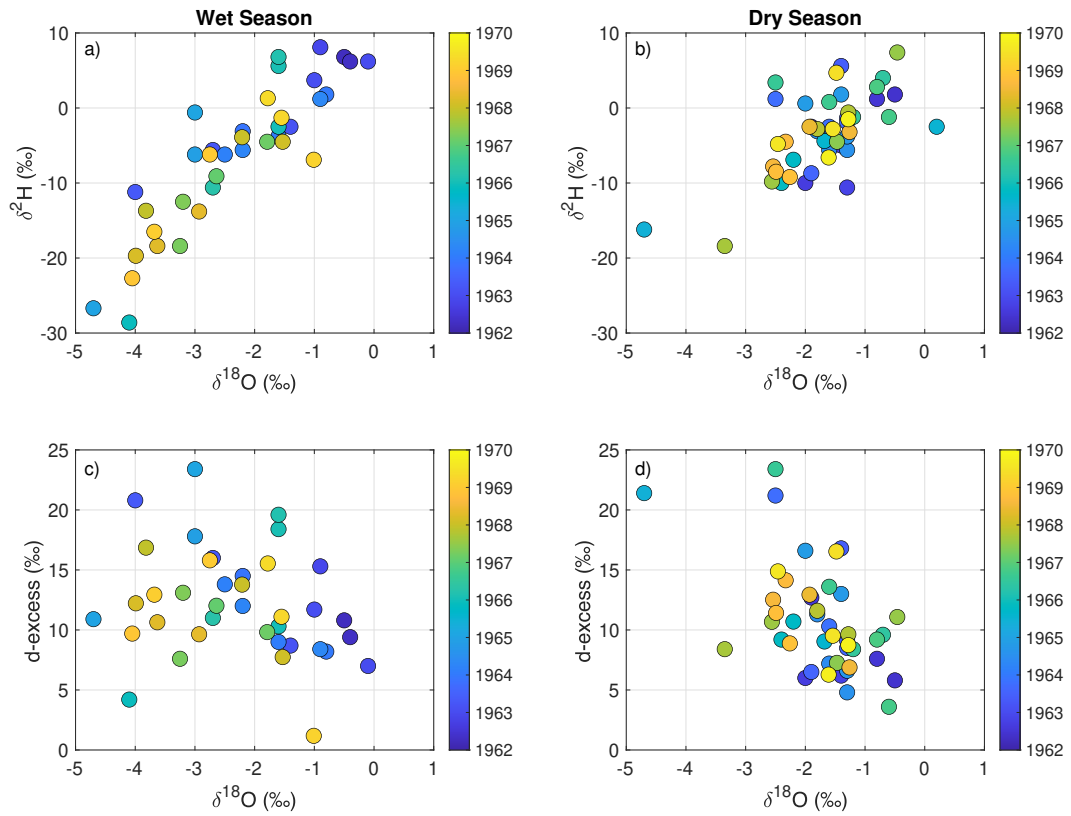


Figure 10. $\delta^{18}\text{O}$ values and deuterium excess for wet season (a,c) and dry season (b,d) shown as a function of $\delta^2\text{H}$ values for the GNIP data at Hilo. Colors reflect the year and the month when data were collected.

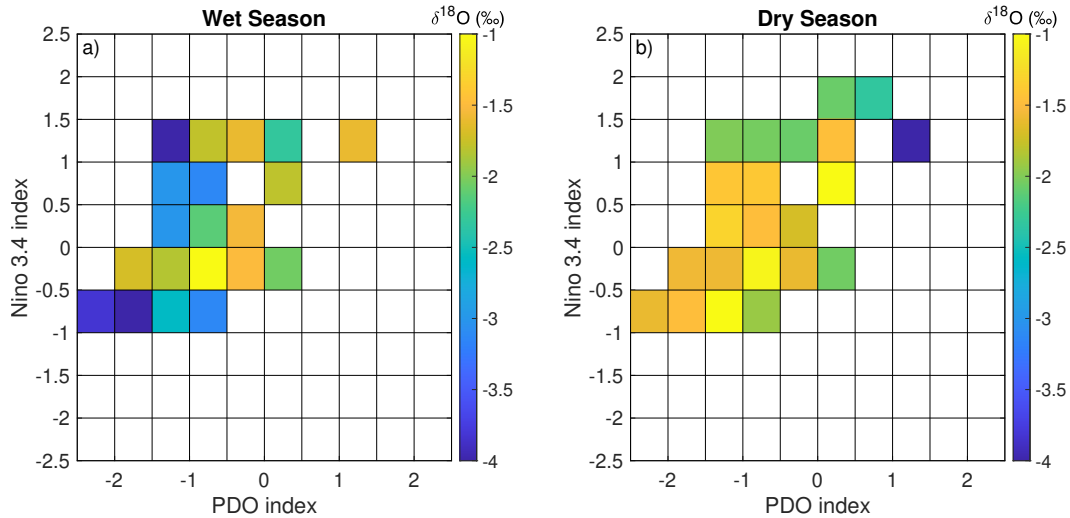


Figure 11. Average $\delta^{18}\text{O}$ for wet-season (a) and dry-season (b) rainfall GNIP data grouped based on the Niño 3.4 and PDO indices at the time when data were collected.

566 interpreted as due to changes in the kinds of systems that bring rainfall to Hawai‘i: years
 567 with lower $\delta^{18}\text{O}$ and $\delta^2\text{H}$ values in wet-season rainfall are characterized by more synop-
 568 tic systems, like Kona lows and cold fronts. This is also consistent with the fact that wet
 569 seasons with lower rainfall $\delta^{18}\text{O}$ and $\delta^2\text{H}$ values are also associated with less accumu-
 570 lated precipitation (not shown).

571 Another way of exploring the interannual variability of rainfall isotopic composi-
 572 tion is through large-scale modes of variability, such as ENSO and the PDO, which have
 573 been shown to influence precipitation in Hawai‘i (Chu & Chen, 2005). Figure 11a and
 574 11b show average $\delta^{18}\text{O}$ values for the wet and dry season, respectively, as functions of
 575 the Niño 3.4 index (*The Climate Data Guide: Niño SST Indices (Niño 1+2, 3, 3.4, 4;*
 576 *ONI and TNI).*, 2021) and the NCEI PDO index (*NCEI PDO Index*, 2021). The fig-
 577 ure suggests a possible correlation between the isotopic composition of rainfall in the wet
 578 season and the PDO, with positive phases being associated with higher $\delta^{18}\text{O}$ and $\delta^2\text{H}$
 579 values. In the case of wet-season rainfall, there does not appear to be a strong correla-
 580 tion with Niño 3.4 index. For the dry season, on the other hand, there appears to be some
 581 correlation with ENSO, with El Niño phases being associated with more lower rainfall
 582 $\delta^{18}\text{O}$ and $\delta^2\text{H}$ values, but not so much with respect to the PDO. The above analysis is
 583 not meant to show rigorous evidence of a clear relationship between rainfall isotopes and
 584 ENSO or the PDO, but, merely to provide a suggestion that such a relationship might
 585 exist, and more work is needed. This would be a particularly significant finding, for ex-
 586 ample, since most of the data collection in Hawai‘i that has been used to compute LMWLs
 587 and estimate aquifer recharge times is typically limited to one or two years. As Putman
 588 et al. (2019) recently pointed out, however, the correct determination of a LMWL in any
 589 particular region requires a collection on time scales at least as long as those of the pro-
 590 cesses controlling the variability. In the case of Hawai‘i, this could imply the necessity
 591 of time series that span multiple years, possibly decades.

592 The increased collection frequency of the data presented in this manuscript rep-
 593 resents an improvement with respect to data previously collected in Hawai‘i, and it al-
 594 lows a clearer understanding of the isotopic composition and the origin of the systems
 595 responsible for precipitation on the islands. At the same time, there are three main lim-
 596 itations to this study. The first is that weekly collections might not be sufficient to make
 597 the data useful for process-based studies, for example to determine rain evaporation frac-

tion, or to assess what causes differences in the isotopic composition of trade-wind rainfall. Another limitation is that the network of sites is quite spatially limited and, given how much $\delta^{18}\text{O}$ and $\delta^2\text{H}$ values as well as deuterium excess can vary within the network, it leaves the open question of the spatial variability across the island of O‘ahu and, more generally, the Hawaiian Archipelago. Finally, the interannual variability suggests that even a 2-year collection might be insufficient to obtain a clear picture of rainfall water isotopic composition in Hawai‘i. Maintaining a long-time data collection over an extended region is very challenging, particularly at this historic time, but efforts are underway to overcome the limitations and increase the potential of the isotope network in Hawai‘i that has been established.

5 Conclusions

The $\delta^{18}\text{O}$ and $\delta^2\text{H}$ values have long been used in climate science to study, for example, past conditions on Earth, the groundwater hydrology in a given location, or, particularly in recent times, atmospheric processes and dynamics. In Hawai‘i, the water isotopic composition has been measured at different times, but most data were either collected at a time when other meteorological data were not available, or at a frequency that was too coarse to allow for a clear interpretation of the signal in terms of the weather systems responsible for rainfall. Here, a new dataset of rainfall $\delta^{18}\text{O}$ and $\delta^2\text{H}$ values is presented based on 2-year collections that started on the island of O‘ahu in 2019, proceeded at nearly-weekly frequency, and is still ongoing.

Compared to previous datasets, the increased frequency used for this study allowed for stronger constraints on the isotopic composition of the precipitating systems that affect the Hawaiian islands. Kona lows, subtropical storms that happen predominantly during the wet season, appear to be responsible for the lowest $\delta^{18}\text{O}$ and $\delta^2\text{H}$ values in rainfall. On the other hand, precipitation from cold fronts, another example of wet-season synoptic systems, presented higher values, and trade-wind showers produced rainfall with the highest $\delta^{18}\text{O}$ and $\delta^2\text{H}$ values. The isotopic composition of rainfall was found to be relatively similar across the network, except for the southernmost sites, where rain tended to have higher $\delta^{18}\text{O}$ and $\delta^2\text{H}$ values and a lower deuterium excess than the other sites, particularly during the dry season. This was interpreted as due to rain evaporation that happens as precipitating systems move across the island and encounter much drier conditions below cloud base on the leeward side, away from the Ko‘olau Range.

The data also showed a significant seasonal cycle in the deuterium excess measured at all five sites. Using trajectory analysis, the difference between wet- and dry-season deuterium excess was explained in terms of the origins of the air masses that are responsible for precipitation: during the winter months, air tends to originate at greater latitudes over the Central/West North Pacific, whereas during the summer months, air originates near the quasi-stationary high-pressure center northeast of the Hawaiian islands. Because deuterium excess in water vapor is related to SST and relative humidity at the source, differences between the two parts of the basin where rain originates were hypothesized to give rise to air masses with different deuterium excesses, which, ultimately, would manifest themselves as differences in the deuterium excess of rainfall.

Finally, the LMWL was computed and compared to previous LMWLs determined on O‘ahu and on other Hawaiian islands. Through simple sub-sampling of the data, it was shown that the LMWL is highly sensitive to the periods chosen to compute it. In order to provide a better assessment of the interannual variability of rainfall $\delta^{18}\text{O}$ and $\delta^2\text{H}$ values in Hawai‘i, the GNIP data from Hilo were examined. The analysis showed significant variations in the isotopic composition of wet-season rainfall and more modest variations during the dry season. The data were then compared with PDO and ENSO indices, and it was shown that wet-season rainfall shows some correlation with the for-

mer, whereas dry-season rainfall appears correlated with the latter. A much longer collection, however, is needed in order to provide more robust results.

Acknowledgments

We would like to express our gratitude to the staff of the Lyon Arboretum for granting us the permission to collect water on their grounds, and for working with us during the COVID-19 pandemic, even at times when the arboretum was closed to the public. We would also like to thank Creighton Litton, John Bravender, Nicole C. Popp, and Jan Reichelderfer for generously agreeing to help in collecting weekly rainfall samples. The data collection would have been impossible without all the passion and hard work that undergraduate students in the Department of Atmospheric Sciences Britt Seifert, Eleanore Law, and John (Jack) Fast put into this project, and to them goes our most heartfelt gratitude. The technical support and advanced computing resources from University of Hawai'i Information Technology Services – Cyberinfrastructure, funded in part by the National Science Foundation MRI award number 1920304, are also gratefully acknowledged. Finally, we want to thank Ryan Longman, Thomas Giambelluca, Yin-Phan Tsang, and Peter Huybers for enlightening discussions. G.T. was partially supported by the National Science Foundation Grant AGS-1945972. The undergraduate students and the equipment purchased for this project were supported by the Undergraduate Research Opportunities Program at the University of Hawai'i at Mānoa. The data used in this paper are available at (link to a Zenodo repository will be provided upon acceptance of the paper). This is SOEST contribution number (the number will be provided upon acceptance).

References

- Adkison, C., Cooper-Norris, C., Patankar, R., & Moore, G. W. (2020). Using high-frequency water vapor isotopic measurements as a novel method to partition daily evapotranspiration in an oak woodland. *Water*, *12*(11). Retrieved from <https://www.mdpi.com/2073-4441/12/11/2967> doi: 10.3390/w12112967
- Aemisegger, F., Pfahl, S., Sodemann, H., Lehner, I., Seneviratne, S. I., & Wernli, H. (2014). Deuterium excess as a proxy for continental moisture recycling and plant transpiration. *Atmospheric Chemistry and Physics*, *14*(8), 4029–4054. Retrieved from <https://acp.copernicus.org/articles/14/4029/2014/> doi: 10.5194/acp-14-4029-2014
- Araguás-Araguás, L., Froehlich, K., & Rozanski, K. (2000). Deuterium and oxygen-18 isotope composition of precipitation and atmospheric moisture. *Hydrological Processes*, *14*(8), 1341-1355. Retrieved from <https://onlinelibrary.wiley.com/doi/abs/10.1002/1099-1085%2820000615%2914%3A8%3C1341%3A%3AAID-HYP983%3E3.0.CO%3B2-Z> doi: [https://doi.org/10.1002/1099-1085\(20000615\)14:8<1341::AID-HYP983>3.0.CO;2-Z](https://doi.org/10.1002/1099-1085(20000615)14:8<1341::AID-HYP983>3.0.CO;2-Z)
- Aron, P. G., Poulsen, C. J., Fiorella, R. P., & Matheny, A. M. (2019). Stable water isotopes reveal effects of intermediate disturbance and canopy structure on forest water cycling. *Journal of Geophysical Research: Biogeosciences*, *124*(10), 2958-2975. Retrieved from <https://agupubs.onlinelibrary.wiley.com/doi/abs/10.1029/2019JG005118> doi: <https://doi.org/10.1029/2019JG005118>
- Bailey, A., Toohey, D., & Noone, D. (2013). Characterizing moisture exchange between the hawaiian convective boundary layer and free troposphere using stable isotopes in water. *Journal of Geophysical Research: Atmospheres*, *118*(15), 8208-8221. Retrieved from <https://agupubs.onlinelibrary.wiley.com/doi/abs/10.1002/jgrd.50639> doi: 10.1002/jgrd.50639
- Bar-Matthews, M., Ayalon, A., & Kaufman, A. (1997). Late quaternary paleoclimate in the eastern mediterranean region from stable isotope analysis of speleothems at soreq cave, israel. *Quaternary Research*, *47*(2), 155-168.

- 699 Retrieved from <https://www.sciencedirect.com/science/article/pii/S0033589497918834> doi: <https://doi.org/10.1006/qres.1997.1883>
- 700
- 701 Barras, V., & Simmonds, I. (2009). Observation and modeling of stable water iso-
- 702 topes as diagnostics of rainfall dynamics over southeastern australia. *Journal*
- 703 *of Geophysical Research: Atmospheres*, *114*(D23). Retrieved from [https://](https://agupubs.onlinelibrary.wiley.com/doi/abs/10.1029/2009JD012132)
- 704 agupubs.onlinelibrary.wiley.com/doi/abs/10.1029/2009JD012132 doi:
- 705 <https://doi.org/10.1029/2009JD012132>
- 706 Beilman, D. W., Massa, C., Nichols, J. E., Elison Timm, O., Kallstrom, R., &
- 707 Dunbar-Co, S. (2019). Dynamic holocene vegetation and north pacific hy-
- 708 droclimate recorded in a mountain peatland, moloka'i, hawai'i. *Frontiers*
- 709 *in Earth Science*, *7*, 188. Retrieved from [https://www.frontiersin.org/](https://www.frontiersin.org/article/10.3389/feart.2019.00188)
- 710 [article/10.3389/feart.2019.00188](https://www.frontiersin.org/article/10.3389/feart.2019.00188) doi: 10.3389/feart.2019.00188
- 711 Cai, M. Y., Wang, L., Parkes, S. D., Strauss, J., McCabe, M. F., Evans, J. P., &
- 712 Griffiths, A. D. (2015). Stable water isotope and surface heat flux simu-
- 713 lation using isolsm: Evaluation against in-situ measurements. *Journal of*
- 714 *Hydrology*, *523*, 67-78. Retrieved from [https://www.sciencedirect.com/](https://www.sciencedirect.com/science/article/pii/S0022169415000360)
- 715 [science/article/pii/S0022169415000360](https://www.sciencedirect.com/science/article/pii/S0022169415000360) doi: [https://doi.org/10.1016/](https://doi.org/10.1016/j.jhydrol.2015.01.019)
- 716 [j.jhydrol.2015.01.019](https://doi.org/10.1016/j.jhydrol.2015.01.019)
- 717 Cao, G., Giambelluca, T. W., Stevens, D. E., & Schroeder, T. A. (2007). Inversion
- 718 variability in the hawaiian trade wind regime. *Journal of Climate*, *20*(7), 1145
- 719 - 1160. Retrieved from [https://journals.ametsoc.org/view/journals/](https://journals.ametsoc.org/view/journals/clim/20/7/jcli4033.1.xml)
- 720 [clim/20/7/jcli4033.1.xml](https://journals.ametsoc.org/view/journals/clim/20/7/jcli4033.1.xml) doi: 10.1175/JCLI4033.1
- 721 Chu, P.-S., & Chen, H. (2005). Interannual and interdecadal rainfall variations
- 722 in the hawaiian islands. *Journal of Climate*, *18*(22), 4796 - 4813. Re-
- 723 trieved from [https://journals.ametsoc.org/view/journals/clim/18/](https://journals.ametsoc.org/view/journals/clim/18/22/jcli3578.1.xml)
- 724 [22/jcli3578.1.xml](https://journals.ametsoc.org/view/journals/clim/18/22/jcli3578.1.xml) doi: 10.1175/JCLI3578.1
- 725 *The climate data guide: Nino sst indices (nino 1+2, 3, 3.4, 4; oni and tni)*. (2021).
- 726 [https://climatedataguide.ucar.edu/climate-data/nino-sst-indices-nino-12-3-34-](https://climatedataguide.ucar.edu/climate-data/nino-sst-indices-nino-12-3-34-4-oni-and-tni)
- 727 [4-oni-and-tni](https://climatedataguide.ucar.edu/climate-data/nino-sst-indices-nino-12-3-34-4-oni-and-tni).
- 728 Cluett, A. A., & Thomas, E. K. (2020). Resolving combined influences of in-
- 729 flow and evaporation on western greenland lake water isotopes to inform
- 730 paleoclimate inferences. *Journal of Paleolimnology*, *63*(4), 251–268. Re-
- 731 trieved from <https://doi.org/10.1007/s10933-020-00114-4> doi:
- 732 [10.1007/s10933-020-00114-4](https://doi.org/10.1007/s10933-020-00114-4)
- 733 Craig, H. (1961). Isotopic variations in meteoric waters. *Science*, *133*(3465), 1702-
- 734 1703.
- 735 Cruz, F. W., Karmann, I., Viana, O., Burns, S. J., Ferrari, J. A., Vuille, M.,
- 736 ... Moreira, M. Z. (2005). Stable isotope study of cave percolation wa-
- 737 ters in subtropical brazil: Implications for paleoclimate inferences from
- 738 speleothems. *Chemical Geology*, *220*(3), 245-262. Retrieved from [https://](https://www.sciencedirect.com/science/article/pii/S0009254105001506)
- 739 www.sciencedirect.com/science/article/pii/S0009254105001506 doi:
- 740 <https://doi.org/10.1016/j.chemgeo.2005.04.001>
- 741 Dahinden, F., Aemisegger, F., Wernli, H., Schneider, M., Diekmann, C. J.,
- 742 Ertl, B., ... Pfahl, S. (2021). Disentangling different moisture trans-
- 743 port pathways over the eastern subtropical north atlantic using multi-
- 744 platform isotope observations and high-resolution numerical modelling.
- 745 *Atmospheric Chemistry and Physics Discussions*, *2021*, 1–49. Retrieved
- 746 from <https://acp.copernicus.org/preprints/acp-2021-269/> doi:
- 747 [10.5194/acp-2021-269](https://doi.org/10.5194/acp-2021-269)
- 748 Dansgaard, W. (1964). Stable isotopes in precipitation. *Tellus*, *16*(4), 436-468.
- 749 Retrieved from [https://onlinelibrary.wiley.com/doi/abs/10.1111/](https://onlinelibrary.wiley.com/doi/abs/10.1111/j.2153-3490.1964.tb00181.x)
- 750 [j.2153-3490.1964.tb00181.x](https://onlinelibrary.wiley.com/doi/abs/10.1111/j.2153-3490.1964.tb00181.x) doi: 10.1111/j.2153-3490.1964.tb00181.x
- 751 Dawson, T. E., Mambelli, S., Plamboeck, A. H., Templer, P. H., & Tu, K. P. (2002,
- 752 2021/03/01/). Stable isotopes in plant ecology. , *33*, 507–559. Retrieved from
- 753 <http://www.jstor.org/stable/3069272>

- 754 Delmotte, M., Masson, V., Jouzel, J., & Morgan, V. I. (2000). A seasonal deuterium
755 excess signal at law dome, coastal eastern antarctica: A southern ocean signa-
756 ture. *Journal of Geophysical Research: Atmospheres*, *105*(D6), 7187-7197.
- 757 Dores, D., Glenn, C. R., Torri, G., Whittier, R. B., & Popp, B. N. (2020). Implica-
758 tions for groundwater recharge from stable isotopic composition of precipita-
759 tion in hawai'i during the 2017–2018 la niña. *Hydrological Processes*, *34*(24),
760 4675-4696. Retrieved from [https://onlinelibrary.wiley.com/doi/abs/
761 10.1002/hyp.13907](https://onlinelibrary.wiley.com/doi/abs/10.1002/hyp.13907) doi: <https://doi.org/10.1002/hyp.13907>
- 762 Draxler, R., & Hess, G. (1998, 12). An overview of the hysplit4 modeling system for
763 trajectories, dispersion, and deposition. *Australian Meteorological Magazine*,
764 *47*, 295-308.
- 765 Ehleringer, J. R., & Dawson, T. E. (1992). Water uptake by plants: perspec-
766 tives from stable isotope composition. *Plant, Cell & Environment*, *15*(9),
767 1073-1082. Retrieved from [https://onlinelibrary.wiley.com/doi/abs/
768 10.1111/j.1365-3040.1992.tb01657.x](https://onlinelibrary.wiley.com/doi/abs/10.1111/j.1365-3040.1992.tb01657.x) doi: [https://doi.org/10.1111/
770 j.1365-3040.1992.tb01657.x](https://doi.org/10.1111/
769 j.1365-3040.1992.tb01657.x)
- 770 Evaristo, J., McDonnell, J. J., Scholl, M. A., Bruijnzeel, L. A., & Chun, K. P.
771 (2016). Insights into plant water uptake from xylem-water isotope mea-
772 surements in two tropical catchments with contrasting moisture con-
773 ditions. *Hydrological Processes*, *30*(18), 3210-3227. Retrieved from
774 <https://onlinelibrary.wiley.com/doi/abs/10.1002/hyp.10841> doi:
775 <https://doi.org/10.1002/hyp.10841>
- 776 Fackrell, J. K., Glenn, C. R., Thomas, D., Whittier, R., & Popp, B. N. (2020).
777 Stable isotopes of precipitation and groundwater provide new insight into
778 groundwater recharge and flow in a structurally complex hydrogeologic sys-
779 tem: West hawai'i, usa. *Hydrogeology Journal*, *28*(4), 1191–1207. Re-
780 trieved from <https://doi.org/10.1007/s10040-020-02143-9> doi:
781 [10.1007/s10040-020-02143-9](https://doi.org/10.1007/s10040-020-02143-9)
- 782 Galewsky, J. (2018). Using stable isotopes in water vapor to diagnose relationships
783 between lower-tropospheric stability, mixing, and low-cloud cover near the
784 island of hawaii. *Geophysical Research Letters*, *45*(1), 297-305. Retrieved
785 from [https://agupubs.onlinelibrary.wiley.com/doi/abs/10.1002/
786 2017GL075770](https://agupubs.onlinelibrary.wiley.com/doi/abs/10.1002/2017GL075770) doi: [10.1002/2017GL075770](https://doi.org/10.1002/2017GL075770)
- 787 Galewsky, J., Steen-Larsen, H. C., Field, R. D., Worden, J., Risi, C., & Schneider,
788 M. (2016). Stable isotopes in atmospheric water vapor and applications
789 to the hydrologic cycle. *Reviews of Geophysics*, *54*(4), 809-865. Retrieved
790 from [https://agupubs.onlinelibrary.wiley.com/doi/abs/10.1002/
791 2015RG000512](https://agupubs.onlinelibrary.wiley.com/doi/abs/10.1002/2015RG000512) doi: [10.1002/2015RG000512](https://doi.org/10.1002/2015RG000512)
- 792 Galewsky, J., Strong, M., & Sharp, Z. D. (2007). Measurements of water vapor
793 d/h ratios from mauna kea, hawaii, and implications for subtropical humidity
794 dynamics. *Geophysical Research Letters*, *34*(22). Retrieved from [https://
795 agupubs.onlinelibrary.wiley.com/doi/abs/10.1029/2007GL031330](https://agupubs.onlinelibrary.wiley.com/doi/abs/10.1029/2007GL031330) doi:
796 [10.1029/2007GL031330](https://doi.org/10.1029/2007GL031330)
- 797 Giambelluca, T. W., Chen, Q., Frazier, A. G., Price, J. P., Chen, Y.-L., Chu, P.-S.,
798 ... Delparte, D. M. (2013). Online rainfall atlas of hawai'i. *Bulletin of the*
799 *American Meteorological Society*, *94*(3), 313 - 316. Retrieved from [https://
800 journals.ametsoc.org/view/journals/bams/94/3/bams-d-11-00228.1.xml](https://journals.ametsoc.org/view/journals/bams/94/3/bams-d-11-00228.1.xml)
801 doi: [10.1175/BAMS-D-11-00228.1](https://doi.org/10.1175/BAMS-D-11-00228.1)
- 802 Gingerich, S., & Oki, D. S. (2000). Ground water in hawaii. *U.S. Geological Survey*.
803 *p. 6.*
- 804 Gröning, M., Lutz, H., Roller-Lutz, Z., Kralik, M., Gourcy, L., & Pölsenstein, L.
805 (2012). A simple rain collector preventing water re-evaporation dedicated for
806 18o and 2h analysis of cumulative precipitation samples. *Journal of Hydrol-*
807 *ogy*, *448-449*, 195-200. Retrieved from [https://www.sciencedirect.com/
808 science/article/pii/S0022169412003411](https://www.sciencedirect.com/science/article/pii/S0022169412003411) doi: <https://doi.org/10.1016/>

809 j.jhydrol.2012.04.041

- 810 Grossiord, C., Sevanto, S., Dawson, T. E., Adams, H. D., Collins, A. D., Dickman,
811 L. T., ... McDowell, N. G. (2017). Warming combined with more extreme pre-
812 cipitation regimes modifies the water sources used by trees. *New Phytologist*,
813 *213*(2), 584-596. Retrieved from <https://nph.onlinelibrary.wiley.com/doi/abs/10.1111/nph.14192> doi: <https://doi.org/10.1111/nph.14192>
- 814
815 Guan, H., Zhang, X., Skrzypek, G., Sun, Z., & Xu, X. (2013). Deuterium excess
816 variations of rainfall events in a coastal area of south australia and its relation-
817 ship with synoptic weather systems and atmospheric moisture sources. *Journal*
818 *of Geophysical Research: Atmospheres*, *118*(2), 1123-1138. Retrieved from
819 <https://agupubs.onlinelibrary.wiley.com/doi/abs/10.1002/jgrd.50137>
820 doi: <https://doi.org/10.1002/jgrd.50137>
- 821 Gupta, P., Noone, D., Galewsky, J., Sweeney, C., & Vaughn, B. H. (2009).
822 Demonstration of high-precision continuous measurements of water vapor
823 isotopologues in laboratory and remote field deployments using wavelength-
824 scanned cavity ring-down spectroscopy (ws-crds) technology. *Rapid Com-*
825 *munications in Mass Spectrometry*, *23*(16), 2534-2542. Retrieved from
826 <https://onlinelibrary.wiley.com/doi/abs/10.1002/rcm.4100> doi:
827 <https://doi.org/10.1002/rcm.4100>
- 828 Hahn, M., Jacobs, S. R., Breuer, L., Rufino, M. C., & Windhorst, D. (2021). Vari-
829 ability in tree water uptake determined with stable water isotopes in an african
830 tropical montane forest. *Ecohydrology*, *n/a*(n/a), e2278. Retrieved from
831 <https://onlinelibrary.wiley.com/doi/abs/10.1002/eco.2278> doi:
832 <https://doi.org/10.1002/eco.2278>
- 833 Hartley, T. M., & Chen, Y.-L. (2010). Characteristics of summer trade wind
834 rainfall over oahu. *Weather and Forecasting*, *25*(6), 1797 - 1815. Re-
835 trieved from [https://journals.ametsoc.org/view/journals/wefo/25/](https://journals.ametsoc.org/view/journals/wefo/25/6/2010waf2222328_1.xml)
836 [6/2010waf2222328_1.xml](https://journals.ametsoc.org/view/journals/wefo/25/6/2010waf2222328_1.xml) doi: 10.1175/2010WAF2222328.1
- 837 Hersbach, H., Bell, W., Berrisford, P., Horányi, A., J., M.-S., Nicolas, J., ...
838 Dee, D. (2019, 04). Global reanalysis: goodbye era-interim, hello era5.
839 , 17-24. Retrieved from <https://www.ecmwf.int/node/19027> doi:
840 [10.21957/vf291hehd7](https://doi.org/10.21957/vf291hehd7)
- 841 Hurley, J. V., Galewsky, J., Worden, J., & Noone, D. (2012). A test of the
842 advection-condensation model for subtropical water vapor using stable iso-
843 topologue observations from mauna loa observatory, hawaii. *Journal of*
844 *Geophysical Research: Atmospheres*, *117*(D19). Retrieved from [https://](https://agupubs.onlinelibrary.wiley.com/doi/abs/10.1029/2012JD018029)
845 agupubs.onlinelibrary.wiley.com/doi/abs/10.1029/2012JD018029 doi:
846 [10.1029/2012JD018029](https://doi.org/10.1029/2012JD018029)
- 847 IAEA/WMO. (2021). Global network of isotopes in precipitation. the gnip database.
848 *Accessible at: http://www.iaea.org/water.*
- 849 Jouzel, J., Stiévenard, M., Johnsen, S., Landais, A., Masson-Delmotte, V., Svein-
850 bjornsdottir, A., ... White, J. (2007). The grip deuterium-excess record.
851 *Quaternary Science Reviews*, *26*(1), 1-17. Retrieved from [https://](https://www.sciencedirect.com/science/article/pii/S0277379106002575)
852 www.sciencedirect.com/science/article/pii/S0277379106002575 doi:
853 <https://doi.org/10.1016/j.quascirev.2006.07.015>
- 854 Kelly, J. L., & Glenn, C. R. (2015). Chlorofluorocarbon apparent ages of ground-
855 waters from west hawaii, usa. *Journal of Hydrology*, *527*, 355-366. Re-
856 trieved from [https://www.sciencedirect.com/science/article/pii/](https://www.sciencedirect.com/science/article/pii/S0022169415003285)
857 [S0022169415003285](https://www.sciencedirect.com/science/article/pii/S0022169415003285) doi: <https://doi.org/10.1016/j.jhydrol.2015.04.069>
- 858 Kodama, K., & Barnes, G. M. (1997). Heavy rain events over the south-
859 facing slopes of hawaii: Attendant conditions. *Weather and Forecasting*,
860 *12*(2), 347 - 367. Retrieved from [https://journals.ametsoc.org/view/](https://journals.ametsoc.org/view/journals/wefo/12/2/1520-0434_1997_012_0347_hreots_2_0_co_2.xml)
861 [journals/wefo/12/2/1520-0434_1997_012_0347_hreots_2_0_co_2.xml](https://journals.ametsoc.org/view/journals/wefo/12/2/1520-0434_1997_012_0347_hreots_2_0_co_2.xml) doi:
862 [10.1175/1520-0434\(1997\)012<0347:HREOTS>2.0.CO;2](https://doi.org/10.1175/1520-0434(1997)012<0347:HREOTS>2.0.CO;2)

- 863 Kodama, K. R., & Businger, S. (1998). Weather and forecasting challenges in
 864 the pacific region of the national weather service. *Weather and Forecasting*,
 865 *13*(3), 523 - 546. Retrieved from [https://journals.ametsoc.org/view/](https://journals.ametsoc.org/view/journals/wefo/13/3/1520-0434-1998_013_0523_wafcit_2_0_co_2.xml)
 866 journals/wefo/13/3/1520-0434-1998_013_0523_wafcit_2_0_co_2.xml doi:
 867 10.1175/1520-0434(1998)013<0523:WAFKIT>2.0.CO;2
- 868 Kontakiotis, G. (2016). Late quaternary paleoenvironmental reconstruction and
 869 paleoclimatic implications of the aegean sea (eastern mediterranean) based on
 870 paleoceanographic indexes and stable isotopes. *Quaternary International*, *401*,
 871 28-42. Retrieved from [https://www.sciencedirect.com/science/article/](https://www.sciencedirect.com/science/article/pii/S1040618215007156)
 872 [pii/S1040618215007156](https://www.sciencedirect.com/science/article/pii/S1040618215007156) (Implications for Late Quaternary Sea Level
 873 Changes on the Mediterranean and Black Sea Coasts - MEDBLACKS2014)
 874 doi: <https://doi.org/10.1016/j.quaint.2015.07.039>
- 875 Kopec, B. G., Feng, X., Posmentier, E. S., & Sonder, L. J. (2019). Seasonal deu-
 876 terium excess variations of precipitation at summit, greenland, and their clima-
 877 tological significance. *Journal of Geophysical Research: Atmospheres*, *124*(1),
 878 72-91. Retrieved from [https://agupubs.onlinelibrary.wiley.com/doi/](https://agupubs.onlinelibrary.wiley.com/doi/abs/10.1029/2018JD028750)
 879 [abs/10.1029/2018JD028750](https://agupubs.onlinelibrary.wiley.com/doi/abs/10.1029/2018JD028750) doi: <https://doi.org/10.1029/2018JD028750>
- 880 Lai, C.-T., & Ehleringer, J. R. (2011). Deuterium excess reveals diurnal sources of
 881 water vapor in forest air. *Oecologia*, *165*(1), 213-223. Retrieved from [https://](https://doi.org/10.1007/s00442-010-1721-2)
 882 doi.org/10.1007/s00442-010-1721-2 doi: 10.1007/s00442-010-1721-2
- 883 LeGrande, A. N., & Schmidt, G. A. (2009). Sources of holocene variability of oxy-
 884 gen isotopes in paleoclimate archives. *Climate of the Past*, *5*(3), 441-455. Re-
 885 trieved from <https://cp.copernicus.org/articles/5/441/2009/> doi: 10
 886 .5194/cp-5-441-2009
- 887 Longman, R. J., Timm, O. E., Giambelluca, T. W., & Kaiser, L. (2021). A 20-year
 888 analysis of disturbance-driven rainfall on o'ahu, hawai'i. *Monthly Weather Re-*
 889 *view*, *149*(6), 1767 - 1783. Retrieved from [https://journals.ametsoc.org/](https://journals.ametsoc.org/view/journals/mwre/149/6/MWR-D-20-0287.1.xml)
 890 [view/journals/mwre/149/6/MWR-D-20-0287.1.xml](https://journals/mwre/149/6/MWR-D-20-0287.1.xml) doi: 10.1175/MWR-D-20
 891 -0287.1
- 892 Lovelock, C. E., Reef, R., & Ball, M. C. (2017). Isotopic signatures of stem water re-
 893 veal differences in water sources accessed by mangrove tree species. *Hydrobiolo-*
 894 *gia*, *803*(1), 133-145. Retrieved from [https://doi.org/10.1007/s10750-017-](https://doi.org/10.1007/s10750-017-3149-8)
 895 [3149-8](https://doi.org/10.1007/s10750-017-3149-8) doi: 10.1007/s10750-017-3149-8
- 896 Mantua, N. J., Hare, S. R., Zhang, Y., Wallace, J. M., & Francis, R. C. (1997).
 897 A pacific interdecadal climate oscillation with impacts on salmon produc-
 898 tion*. *Bulletin of the American Meteorological Society*, *78*(6), 1069 - 1080.
 899 Retrieved from [https://journals.ametsoc.org/view/journals/bams/](https://journals.ametsoc.org/view/journals/bams/78/6/1520-0477_1997_078_1069_apicow_2_0_co_2.xml)
 900 [78/6/1520-0477_1997_078_1069_apicow_2_0_co_2.xml](https://journals/bams/78/6/1520-0477_1997_078_1069_apicow_2_0_co_2.xml) doi: 10.1175/
 901 1520-0477(1997)078<1069:APICOW>2.0.CO;2
- 902 Marshall, J. D., Brooks, J. R., & Lajtha, K. (2007). Sources of variation in the
 903 stable isotopic composition of plants. In *Stable isotopes in ecology and en-*
 904 *vironmental science* (p. 22-60). John Wiley Sons, Ltd. Retrieved from
 905 <https://onlinelibrary.wiley.com/doi/abs/10.1002/9780470691854.ch2>
 906 doi: <https://doi.org/10.1002/9780470691854.ch2>
- 907 Massa, C., Beilman, D. W., Nichols, J. E., & Timm, O. E. (2021). Central pa-
 908 cific hydroclimate over the last 45,000 years: Molecular-isotopic evidence from
 909 leaf wax in a hawaii peatland. *Quaternary Science Reviews*, *253*, 106744.
 910 Retrieved from [https://www.sciencedirect.com/science/article/pii/](https://www.sciencedirect.com/science/article/pii/S027737912030706X)
 911 [S027737912030706X](https://www.sciencedirect.com/science/article/pii/S027737912030706X) doi: <https://doi.org/10.1016/j.quascirev.2020.106744>
- 912 Masson-Delmotte, V., Jouzel, J., Landais, A., Stievenard, M., Johnsen, S. J., White,
 913 J. W. C., ... Fuhrer, K. (2005). Grip deuterium excess reveals rapid and
 914 orbital-scale changes in greenland moisture origin. *Science*, *309*(5731), 118-
 915 121.
- 916 Merlivat, L., & Jouzel, J. (1979). Global climatic interpretation of the
 917 deuterium-oxygen 18 relationship for precipitation. *Journal of Geophys-*

- 918 *ical Research: Oceans*, 84(C8), 5029-5033. Retrieved from [https://](https://agupubs.onlinelibrary.wiley.com/doi/abs/10.1029/JC084iC08p05029)
 919 agupubs.onlinelibrary.wiley.com/doi/abs/10.1029/JC084iC08p05029
 920 doi: <https://doi.org/10.1029/JC084iC08p05029>
- 921 *Ncei pdo index*. (2021). <https://www.ncdc.noaa.gov/teleconnections/pdo/>.
- 922 Noone, D., Galewsky, J., Sharp, Z. D., Worden, J., Barnes, J., Baer, D., ... Wright,
 923 J. S. (2011). Properties of air mass mixing and humidity in the subtrop-
 924 ics from measurements of the d/h isotope ratio of water vapor at the mauna
 925 loa observatory. *Journal of Geophysical Research: Atmospheres*, 116(D22).
 926 Retrieved from [https://agupubs.onlinelibrary.wiley.com/doi/abs/](https://agupubs.onlinelibrary.wiley.com/doi/abs/10.1029/2011JD015773)
 927 [10.1029/2011JD015773](https://agupubs.onlinelibrary.wiley.com/doi/abs/10.1029/2011JD015773) doi: 10.1029/2011JD015773
- 928 Opel, T., Meyer, H., Wetterich, S., Laepple, T., Dereviagin, A., & Murton,
 929 J. (2018). Ice wedges as archives of winter paleoclimate: A review.
 930 *Permafrost and Periglacial Processes*, 29(3), 199-209. Retrieved from
 931 <https://onlinelibrary.wiley.com/doi/abs/10.1002/ppp.1980> doi:
 932 <https://doi.org/10.1002/ppp.1980>
- 933 Papritz, L., Aemisegger, F., & Wernli, H. (2021). Sources and transport pathways
 934 of precipitating waters in cold-season deep north atlantic cyclones. *Journal of*
 935 *the Atmospheric Sciences*. Retrieved from [https://journals.ametsoc.org/](https://journals.ametsoc.org/view/journals/atsc/aop/JAS-D-21-0105.1/JAS-D-21-0105.1.xml)
 936 [view/journals/atsc/aop/JAS-D-21-0105.1/JAS-D-21-0105.1.xml](https://journals/ametsoc.org/view/journals/atsc/aop/JAS-D-21-0105.1/JAS-D-21-0105.1.xml) doi: 10
 937 .1175/JAS-D-21-0105.1
- 938 Pfahl, S., & Sodemann, H. (2014). What controls deuterium excess in global pre-
 939 cipitation? *Climate of the Past*, 10(2), 771-781. Retrieved from [https://cp](https://cp.copernicus.org/articles/10/771/2014/)
 940 [.copernicus.org/articles/10/771/2014/](https://cp.copernicus.org/articles/10/771/2014/) doi: 10.5194/cp-10-771-2014
- 941 Pfahl, S., & Wernli, H. (2009). Lagrangian simulations of stable isotopes in wa-
 942 ter vapor: An evaluation of nonequilibrium fractionation in the craig-gordon
 943 model. *Journal of Geophysical Research: Atmospheres*, 114(D20). Retrieved
 944 from [https://agupubs.onlinelibrary.wiley.com/doi/abs/10.1029/](https://agupubs.onlinelibrary.wiley.com/doi/abs/10.1029/2009JD012054)
 945 [2009JD012054](https://agupubs.onlinelibrary.wiley.com/doi/abs/10.1029/2009JD012054) doi: <https://doi.org/10.1029/2009JD012054>
- 946 Putman, A. L., Fiorella, R. P., Bowen, G. J., & Cai, Z. (2019). A global perspec-
 947 tive on local meteoric water lines: Meta-analytic insight into fundamental
 948 controls and practical constraints. *Water Resources Research*, 55(8), 6896-
 949 6910. Retrieved from [https://agupubs.onlinelibrary.wiley.com/doi/abs/](https://agupubs.onlinelibrary.wiley.com/doi/abs/10.1029/2019WR025181)
 950 [10.1029/2019WR025181](https://agupubs.onlinelibrary.wiley.com/doi/abs/10.1029/2019WR025181) doi: <https://doi.org/10.1029/2019WR025181>
- 951 Rozanski, K., Araguás-Araguás, L., & Gonfiantini, R. (1993). Isotopic patterns
 952 in modern global precipitation. In *Climate change in continental isotopic*
 953 *records* (p. 1-36). American Geophysical Union (AGU). Retrieved from
 954 <https://agupubs.onlinelibrary.wiley.com/doi/abs/10.1029/GM078p0001>
 955 doi: <https://doi.org/10.1029/GM078p0001>
- 956 Scholl, M. A., Giambelluca, T. W., Gingerich, S. B., Nullet, M. A., & Loope, L. L.
 957 (2007). Cloud water in windward and leeward mountain forests: The sta-
 958 ble isotope signature of orographic cloud water. *Water Resources Research*,
 959 43(12). Retrieved from [https://agupubs.onlinelibrary.wiley.com/doi/](https://agupubs.onlinelibrary.wiley.com/doi/abs/10.1029/2007WR006011)
 960 [abs/10.1029/2007WR006011](https://agupubs.onlinelibrary.wiley.com/doi/abs/10.1029/2007WR006011) doi: <https://doi.org/10.1029/2007WR006011>
- 961 Scholl, M. A., Gingerich, S. B., & Tribble, G. W. (2002). The influence of micro-
 962 climates and fog on stable isotope signatures used in interpretation of regional
 963 hydrology: East maui, hawaii. *Journal of Hydrology*, 264(1), 170-184. Re-
 964 trieved from [https://www.sciencedirect.com/science/article/pii/](https://www.sciencedirect.com/science/article/pii/S0022169402000732)
 965 [S0022169402000732](https://www.sciencedirect.com/science/article/pii/S0022169402000732) doi: [https://doi.org/10.1016/S0022-1694\(02\)00073-2](https://doi.org/10.1016/S0022-1694(02)00073-2)
- 966 Scholl, M. A., Ingebritsen, S. E., Janik, C. J., & Kauahikaua, J. P. (1996). Use
 967 of precipitation and groundwater isotopes to interpret regional hydrology on
 968 a tropical volcanic island: Kilauea volcano area, Hawaii. *Water Resources*
 969 *Research*, 32(12), 3525-3537. doi: 10.1029/95WR02837
- 970 Simpson, R. H. (1952). Evolution of the kona storm a subtropical cyclone. *Journal*
 971 *of Atmospheric Sciences*, 9(1), 24 - 35. Retrieved from [https://journals](https://journals.ametsoc.org/view/journals/atsc/9/1/1520-0469_1952_009_0024_eotksa)
 972 [.ametsoc.org/view/journals/atsc/9/1/1520-0469_1952_009_0024_eotksa](https://journals.ametsoc.org/view/journals/atsc/9/1/1520-0469_1952_009_0024_eotksa)

- 973 _2.0_co.2.xml doi: 10.1175/1520-0469(1952)009(0024:EOTKSA)2.0.CO;2
- 974 Sodemann, H., Masson-Delmotte, V., Schwierz, C., Vinther, B. M., & Wernli, H.
975 (2008). Interannual variability of greenland winter precipitation sources: 2.
976 effects of north atlantic oscillation variability on stable isotopes in precipita-
977 tion. *Journal of Geophysical Research: Atmospheres*, 113(D12). Retrieved
978 from [https://agupubs.onlinelibrary.wiley.com/doi/abs/10.1029/](https://agupubs.onlinelibrary.wiley.com/doi/abs/10.1029/2007JD009416)
979 2007JD009416 doi: <https://doi.org/10.1029/2007JD009416>
- 980 *State of hawaii data book*. (2004). Hawaii. Dept. of Business, Economic Development
981 and Tourism. Research and Economic Analysis Division. Statistics and Data
982 Support Branch.
- 983 Stein, A. F., Draxler, R. R., Rolph, G. D., Stunder, B. J. B., Cohen, M. D., & Ngan,
984 F. (2015). Noaa's hysplit atmospheric transport and dispersion modeling
985 system. *Bulletin of the American Meteorological Society*, 96(12), 2059 - 2077.
986 Retrieved from [https://journals.ametsoc.org/view/journals/bams/96/](https://journals.ametsoc.org/view/journals/bams/96/12/bams-d-14-00110.1.xml)
987 12/bams-d-14-00110.1.xml doi: 10.1175/BAMS-D-14-00110.1
- 988 Tachera, D. K., Lautze, N. C., Torri, G., & Thomas, D. M. (2021). Charac-
989 terization of the isotopic composition and bulk ion deposition of precipi-
990 tation from central to west hawaii island between 2017 and 2019. *Jour-
991 nal of Hydrology: Regional Studies*, 34, 100786. Retrieved from [https://](https://www.sciencedirect.com/science/article/pii/S221458182100015X)
992 www.sciencedirect.com/science/article/pii/S221458182100015X doi:
993 <https://doi.org/10.1016/j.ejrh.2021.100786>
- 994 Tetzlaff, D., Buttle, J., Carey, S. K., Kohn, M. J., Laudon, H., McNamara, J. P.,
995 ... Soulsby, C. (2021). Stable isotopes of water reveal differences in plant –
996 soil water relationships across northern environments. *Hydrological Processes*,
997 35(1), e14023. Retrieved from [https://onlinelibrary.wiley.com/doi/abs/](https://onlinelibrary.wiley.com/doi/abs/10.1002/hyp.14023)
998 10.1002/hyp.14023 doi: <https://doi.org/10.1002/hyp.14023>
- 999 Tillman, F. D., Oki, D. S., Johnson, A. G., Barber, L. B., & Beisner, K. R.
1000 (2014). Investigation of geochemical indicators to evaluate the connection
1001 between inland and coastal groundwater systems near kaloko-honokōhau
1002 national historical park, hawaii. *Applied Geochemistry*, 51, 278–292. Re-
1003 trieved from [https://www.sciencedirect.com/science/article/pii/](https://www.sciencedirect.com/science/article/pii/S0883292714002352)
1004 S0883292714002352 doi: <https://doi.org/10.1016/j.apgeochem.2014.10.003>
- 1005 Timofeeva, G., Treydte, K., Bugmann, H., Salmon, Y., Rigling, A., Schaub, M., ...
1006 Saurer, M. (2020, 06). How does varying water supply affect oxygen isotope
1007 variations in needles and tree rings of Scots pine? *Tree Physiology*, 40(10),
1008 1366-1380. Retrieved from <https://doi.org/10.1093/treephys/tpaa082>
1009 doi: 10.1093/treephys/tpaa082
- 1010 Trenberth, K. E. (1997). The definition of el niño. *Bulletin of the American
1011 Meteorological Society*, 78(12), 2771 - 2778. Retrieved from [https://](https://journals.ametsoc.org/view/journals/bams/78/12/1520-0477_1997_078_2771_tdoeno_2.0.co_2.xml)
1012 [journals.ametsoc.org/view/journals/bams/78/12/1520-0477_1997](https://journals.ametsoc.org/view/journals/bams/78/12/1520-0477_1997_078_2771_tdoeno_2.0.co_2.xml)
1013 [_078.2771_tdoeno_2.0.co.2.xml](https://journals.ametsoc.org/view/journals/bams/78/12/1520-0477_1997_078_2771_tdoeno_2.0.co_2.xml) doi: 10.1175/1520-0477(1997)078(2771:
1014 TDOENO)2.0.CO;2
- 1015 Uemura, R., Matsui, Y., Yoshimura, K., Motoyama, H., & Yoshida, N. (2008).
1016 Evidence of deuterium excess in water vapor as an indicator of ocean surface
1017 conditions. *Journal of Geophysical Research: Atmospheres*, 113(D19). Re-
1018 trieved from <https://doi.org/10.1029/2008JD010209> doi: [https://doi.org/](https://doi.org/10.1029/2008JD010209)
1019 10.1029/2008JD010209
- 1020 U.S. Census Bureau, P. D. (2020). *Annual estimates of the resident population for
1021 the united states, regions, states, and the district of columbia: April 1, 2010 to
1022 july 1, 2020 (nst-est2020)*.
- 1023 Veron, S., Mouchet, M., Govaerts, R., Haevermans, T., & Pellens, R. (2019). Vulner-
1024 ability to climate change of islands worldwide and its impact on the tree of life.
1025 *Scientific Reports*, 9(1), 14471. Retrieved from [https://doi.org/10.1038/](https://doi.org/10.1038/s41598-019-51107-x)
1026 s41598-019-51107-x doi: 10.1038/s41598-019-51107-x

- 1027 Villiger, L., Wernli, H., Boettcher, M., Hagen, M., & Aemisegger, F. (2021).
1028 Lagrangian formation pathways of moist anomalies in the trade-wind re-
1029 gion during the dry season: two case studies from eurec⁴a. *Weather and*
1030 *Climate Dynamics Discussions, 2021*, 1–49. Retrieved from [https://](https://wcd.copernicus.org/preprints/wcd-2021-42/)
1031 wcd.copernicus.org/preprints/wcd-2021-42/ doi: 10.5194/wcd-2021-42
1032 Vimeux, F., Masson, V., Jouzel, J., Stievenard, M., & Petit, J. R. (1999). Glacial-
1033 interglacial changes in ocean surface conditions in the southern hemisphere.
1034 *Nature, 398*(6726), 410–413. Retrieved from [https://doi.org/10.1038/](https://doi.org/10.1038/18860)
1035 [18860](https://doi.org/10.1038/18860) doi: 10.1038/18860
1036 Woodruff, F., Savin, S. M., & Douglas, R. G. (1981). Miocene stable isotope record:
1037 A detailed deep pacific ocean study and its paleoclimatic implications. *Science,*
1038 *212*(4495), 665–668. Retrieved from [https://science.sciencemag.org/](https://science.sciencemag.org/content/212/4495/665)
1039 [content/212/4495/665](https://science.sciencemag.org/content/212/4495/665) doi: 10.1126/science.212.4495.665
1040 Yao, T., Masson-Delmotte, V., Gao, J., Yu, W., Yang, X., Risi, C., ... Hou, S.
1041 (2013). A review of climatic controls on 18o in precipitation over the tibetan
1042 plateau: Observations and simulations. *Reviews of Geophysics, 51*(4), 525-
1043 548. Retrieved from [https://agupubs.onlinelibrary.wiley.com/doi/abs/](https://agupubs.onlinelibrary.wiley.com/doi/abs/10.1002/rog.20023)
1044 [10.1002/rog.20023](https://agupubs.onlinelibrary.wiley.com/doi/abs/10.1002/rog.20023) doi: <https://doi.org/10.1002/rog.20023>
1045 Yoshimura, K. (2015). Stable water isotopes in climatology, meteorology, and hy-
1046 drology: A review. *J. Meteorol. Soc. Japan, 93*(5), 513–533. doi: 10.2151/jmsj.2015-036
1047 Yoshimura, K., & Ichiyanagi, K. (2009). A reconsideration of seasonal variation in
1048 precipitation deuterium excess over east asia. *Journal of Japan Society of Hy-*
1049 *drology and Water Resources, 22*(4), 262-276.